Oligocene and Miocene TEX$_{86}$-derived seawater temperatures from offshore Wilkes Land (East Antarctica)

Keywords:

TEX$_{86}$

Oligocene

Wilkes Land

sea surface temperature

Antarctic ice sheet

Julian D. Hartman[1], Francesca Sangiorgi[1], Ariadna Salabarnada[2], Francien Peterse[1], Alexander J.P. Houben[3], Stefan Schouten[4], Henk Brinkhuis[1,4], Carlota Escutia[2], Peter K. Bijl[1]

[1] Marine Palynology and Paleoceanography, Laboratory of Palaeobotany and Palynology, Department of Earth Sciences, Utrecht University, Princetonlaan 8a, 3584CB Utrecht, The Netherlands

[2] Instituto Andaluz de Ciencias de la Tierra, CSIC/Universidad de Granada, Avenida de las Palmeras 4, 18100 Armilla, Granada, Spain

[3] Applied Geosciences Team, Netherlands Organisation for applied scientific Research (TNO), Princetonlaan 6, 3584CB Utrecht, The Netherlands

[4] NIOZ Royal Netherlands Institute for Sea Research, and Utrecht University, Landsdiep 4, 1797SZ 't Horntje, Texel, The Netherlands

Correspondence to: Julian D. Hartman (juulhartman@gmail.com)

Abstract. The volume of the Antarctic continental ice sheet(s) varied substantially during the Oligocene and Miocene (~34-5 Ma) from smaller to substantially larger than today, both on million-year and on orbital timescales. However, reproduction through physical modeling of a dynamic response of the ice sheets to climate forcing remains problematic, suggesting the existence of complex feedbacks between cryosphere, the ocean and the atmosphere systems. There is therefore an urgent need to improve the models for better predictions of these systems, including resulting potential future sea level change. To assess the interactions between cryosphere, ocean and atmosphere, knowledge of ancient sea surface conditions close to the Antarctic margin is essential. Here, we present a new TEX_{86}-based sea surface water paleotemperature record measured on Oligocene sediments from Integrated Ocean Drilling Program (IODP) Site U1356, offshore Wilkes Land, East Antarctica. The new data is presented along with previously published Miocene temperatures from the same site. Together the data covers the interval between ~34 to ~11 Ma and encompasses 2 hiatuses. This record allows us to accurately reconstruct the magnitude of sea surface temperature (SST) variability and trends on both million-year and on glacial-interglacial timescales. On average, TEX_{86} values indicate SSTs ranging between 10 and 21°C during the Oligocene and Miocene, which is on the upper end of the few existing reconstructions from other high-latitude Southern Ocean Sites. SST maxima occur around 30.5, 25 and 17 Ma. Our record suggests generally warm to temperate ocean offshore Wilkes Land. Based on lithological alternations detected in the sedimentary record, which are assigned to glacial-interglacial deposits, a SST variability of 1.5–3.1°C at glacial-interglacial timescales can be established. This variability is slightly larger than that of deep-sea temperatures recorded in Mg/Ca data. Our reconstructed Oligocene temperature variability has implications for Oligocene ice-volume estimates based on benthic $\delta^{18}O$ records. If the long-term and orbital-scale SST variability at Site U1356 mirrors that of the nearby region of deep-water formation, we argue that a substantial portion of the variability and trends contained in long-term $\delta^{18}O$ records can be explained by variability in Southern high-latitude temperature and that the Antarctic ice volume may have been less dynamic than previously thought. Importantly, our temperature record suggests that Oligocene-Miocene Antarctic ice sheets were generally of smaller size compared to today.

1 Introduction

50 Numerical paleoclimate models predict that with the current rate of ice volume loss (up to 109±56 Gt/yr, The IMBRIE Team, 2018) several sectors of the West Antarctic marine-based ice sheet will disappear within the coming few centuries (e.g., Joughin et al. 2014; The IMBRIE Team, 2018) favored by ocean warming-induced collapse. Observations show that glaciers on East Antarctica are also vulnerable to basal melt through warming of the ocean waters when they are grounded below sea level (Greenbaum et al., 2015; Miles et al., 2016; Shen et al., 2018; The

55 IMBRIE Team, 2018), making the East Antarctic ice sheet (EAIS) not as stable as previously thought (Mcmillan et al., 2014). Recent numerical modelling studies have improved on reproducing the observed ice-sheet volume decrease, as they incorporate positive feedbacks (e.g., bedrock topography) to global warming and more complicated physics (e.g., hydrofracturing and ice-cliff failure) into these models (Austermann et al., 2015; Deconto and Pollard, 2016; Fogwill et al., 2014; Golledge et al., 2017; Pollard et al., 2015). They indeed show that sensitivity

60 to global warming is particularly high where the ice sheet is grounded below sea level (Fretwell et al., 2013), such as in the Wilkes Land basin (Golledge et al., 2017; Shen et al., 2018).

Both on glacial-interglacial (Parrenin et al., 2013) and longer term Cenozoic timescales (Pagani et al., 2011; Zachos et al., 2008), Antarctic ice-volume changes have been mostly linked to changes in atmospheric CO_2 concentrations (pCO_2, see e.g., Foster & Rohling 2013; Crampton et al. 2016), modulated by astronomically forced changes in

65 insolation (e.g., Holbourn et al., 2013; Liebrand et al., 2017; Miller et al., 2017; Pälike et al., 2006b; Westerhold et al., 2005). Foster & Rohling (2013) compiled pCO_2 proxy data and associated sea level reconstructions for the last 40 million years (Myr). These data suggest that if the past is projected to the future all ice on West Antarctica and Greenland may be lost under current and near future atmospheric CO_2 conditions (400-450 ppmv) in equilibrium state. Projections of pCO_2 for future emission scenarios of the latest IPCC Report (2014) show a range from 500 to

70 1000 ppmv for the year 2100, which could lead to additional ice-sheet volume loss from East Antarctica. This range in atmospheric pCO_2 is similar to that reconstructed for the warmest intervals of the Oligocene and Miocene epochs (full range: 200–1000 ppmv; e.g., Zhang et al. 2013). Given that observations clearly link the recent instability of marine-based ice sheets to ocean warming, it becomes important to better constrain near-field sea surface temperatures (SSTs) from the Antarctic margin during the Oligocene and Miocene to improve our understanding of

75 past ice sheet dynamics and the projections for the future.

EAIS volume changes have been suggested for the Oligocene and Miocene based on a number of deep-sea $\delta^{18}O$ records, which reflect a combination of bottom-water temperature and ice volume (e.g., Liebrand et al., 2017; Miller et al., 2013; Pekar et al., 2006; Pekar and Christie-Blick, 2008; Shevenell et al., 2004; Westerhold et al., 2005), as well as sedimentary paleosealevel reconstructions (John et al., 2011; Gallagher et al., 2013; Stap et al., 2017). These

80 records show long-term (1-3 Myr) trends punctuated by strong but transient glaciation events (Oi- and Mi-events) (Hauptvogel et al., 2017; Miller et al., 2017; Liebrand et al., 2017, 2016; Pälike et al., 2006b; Westerhold et al., 2005). Following the onset of the Oligocene, marked by the Oi-1 glaciation event, the long-term trend shows a shift towards lighter $\delta^{18}O$ values and a steady increase towards 27 Ma, then a decrease to 24 Ma and a final increase leading into the Miocene, marked by the Mi-1 glaciation event (Beddow et al., 2016; Cramer et al., 2009; Liebrand

85 et al., 2016; Zachos, 2001). Miocene benthic $\delta^{18}O$ long-term trends show a sudden increase at 16.9 Ma, which marks

the onset of the Miocene Climatic Optimum (MCO), a plateau phase, and a subsequent stepwise decrease known as the mid-Miocene Climatic Transition (MCT) (Holbourn et al., 2015, 2013, 2007; Shevenell et al., 2004; Westerhold et al., 2005). The Oligocene and Miocene glaciations are paced by periods of strong 110-kyr eccentricity fluctuations of up to 1‰ (Liebrand et al., 2017, 2016, 2011). These $\delta^{18}O$ fluctuations may be mostly resulting from

90   the waxing and waning of the EAIS, in which case the ice sheet was highly dynamic, or they mostly reflect large changes in deep-sea temperature, in which case large SST fluctuations in the region of deep-water formation were to be expected. Considering the former, fluctuations between 50% and 125% of the present-day EAIS have been suggested for the Oligocene (DeConto et al., 2008; Pekar et al., 2006; Pekar and Christie-Blick, 2008), but this amount of variability has not yet been entirely reproduced by numerical modeling studies (DeConto et al., 2008;

95   Gasson et al., 2016; Pollard et al., 2015). Considering the latter, several studies have suggested that during the Oligocene the southern high latitudes were the prevalent source for cold deep-water formation (Katz et al. 2011; Goldner et al. 2014; Borelli & Katz 2015). Hence, deep-water temperature records from the southern high-latitudes, particularly those capturing temperature changes on million-year as well as orbital timescales, may provide information on the relative contribution of deep-sea temperature variability to the $\delta^{18}O$ records. However,

100   reconstructions of deep-water temperature based on $\delta^{18}O$ and Mg/Ca ratios of benthic foraminifera are hampered by the poor preservation of carbonates on the high-latitude Southern Ocean floor, and rely on critical assumptions on past composition of seawater chemistry. Therefore, one needs to assume that the deep-sea temperature trend captured in the Oligocene and Miocene $\delta^{18}O$ records is related to surface water temperature in the Southern Ocean similarly to today (Baines, 2009; Jacobs, 1991) and in the Eocene (Bijl et al., 2009). Based on this assumption,

105   Southern Ocean SSTs would potentially gauge deep-sea temperature variability. Only few Oligocene SST estimates are available for the Southern Ocean and they relate to the early Oligocene (Petersen and Schrag, 2015; Plancq et al., 2014). Few Southern Ocean SST records are available for the early and mid-Miocene (14–17 Ma) (Kuhnert et al., 2009; Majewski & Bohaty, 2010; Shevenell et al., 2004) and only two (Levy et al., 2016; Sangiorgi et al., 2018) are derived from south of the Polar Front (PF). Obstacles for reconstructing Oligocene and Miocene SST in the

110   Southern Ocean are the paucity of stratigraphically well-calibrated sedimentary archives, as well as suitable indicator fossils/compounds within these sediments that can be used to reconstruct SST.
In 2010, the Integrated Ocean Drilling Program (IODP) cored a sedimentary archive at the boundary of the continental rise and the abyssal plain offshore Wilkes Land with a well-dated Oligocene and Miocene sequence: IODP Site U1356 (Fig. 1), suitable for paleoclimatological analysis. In this study we use the now well-established

115   ratio between several isoprenoidal glycerol dialkyl glycerol tetraethers (GDGTs), the so-called TEX_{86} proxy (Schouten et al., 2013, 2002), to reconstruct SSTs at this high-latitude Southern Ocean site. We present new SST data based on TEX_{86}, covering almost the entire Oligocene, along with published TEX_{86} values for the mid-Miocene section (Sangiorgi et al., 2018). Detailed lithological logging of both the Oligocene and Miocene sections of Site U1356 allows for the distinction of glacial and interglacial deposits (Salabarnada et al., submitted this volume). This

120   enables us to assess long-term evolution of SSTs in proximity of the ice-sheet as well as the temperature differences between glacials and interglacials on orbital time scales, which have implications on the dynamics of the Antarctic ice-sheet and its sensitivity to climate change. We compare our record with the few existing early Oligocene and

mid-Miocene SST data from other high latitude Southern Ocean sites as well as with deep-water δ^{18}O and Mg/Ca-based bottom water temperature (BWT) records from lower latitudes (Billups & Schrag 2002; Lear et al., 2004;
125 Shevenell et al., 2004), and discuss the implications of our findings.

2 Materials & Methods

2.1 Site description

Integrated Ocean Drilling Program (IODP) Expedition 318 Site U1356 was cored about 300 kilometers off the Wilkes Land coast (63°54.61'S, 135°59.94'E) at the boundary between the continental rise and the abyssal plain at a
130 water depth of 3992 m (Escutia et al. 2011, see Fig. 1). Today, this site is south of the Antarctic Polar Front (PF) and is under the influence of by Antarctic Bottom Waters (AABW), Lower Component Deep Water (LCDW), Upper Component Deep Water (UCDW), and Antarctic Surface Water (AASW) (Orsi et al., 1995).

2.2 Sedimentology

At present, IODP Site U1356 receives sediments transported from the shelf and the slope as well as *in situ* pelagic
135 component. Although we have no quantitative constraints on the water depth during the Oligocene and Miocene, the sediments as well as the biota suggest a deep-water setting at Site U1356 during these times (Houben et al., 2013; Escutia et al., 2014). Sedimentary Units of Hole U1356A have been defined in the shipboard report (Escutia et al., 2011). Detailed logging of the sediments recovered in Hole U1356A has revealed that the Oligocene and Miocene sedimentary record (between 95.40 and 894.80 meters below sea floor, mbsf) consists mostly of alternations of
140 (diatomaceous) laminated and bioturbated sediments, gravity flow deposits, and carbonate beds (Salabarnada et al., submitted this volume; Sangiorgi et al., 2018) (Fig. 2). Gravity flow deposits include Mass Transport Deposits (MTDs) formed by the slump and debris flow sediments of the Miocene, Oligocene and Eocene-Oligocene Transition (EOT), and the late Oligocene-Miocene turbidite type facies as defined by Salabarnada et al. (submitted this volume). Samples from the MTDs contain the largest contribution of reworked older material transported from
145 the continental shelf (Bijl et al., submitted this volume), while in the other lithologies, this component is much more reduced or absent.

Between 593.4 and 795.1 mbsf, there are clear alternations between greenish carbonate-poor laminated and grey bioturbated deposits with some carbonate-rich bioturbated intervals. These deposits are interpreted as contourite deposits recording glacial-interglacial environmental variability (Salabarnada et al., submitted this volume). Above
150 600 mbsf, sediments mostly consist of MTDs with low to abundant clasts (Fig. 2). However, between the MTDs greenish or grey laminated deposits and greenish or grey bioturbated deposits are preserved. Near the bottom of Unit III as defined in the shipboard report (around 433 mbsf and below), a different depositional setting is represented with alternations between pelagic clays and (ripple) cross-laminated sandstone beds (Escutia et al., 2011). These sandy (ripple) cross-laminated beds are interpreted as turbidite deposits (Salabarnada et al., submitted this volume).
155 Above these turbidite deposits, there are diatomaceous silty clays that are characterized by an alternation of green

laminated and grey homogeneous (bioturbated) silty clays. Apart from their diatom content, these deposits are very similar to the Oligocene alternations between carbonate-poor laminated and carbonate-containing bioturbated deposits, and are therefore interpreted likewise (Salabarnada et al., submitted this volume). Upcore within the Miocene section, the alternations between laminated and homogeneous diatomaceous silty clays become more frequent. In the upper Miocene sections (95.4–110 mbsf) laminations become less clear as the sediments become less consolidated, however green and grey alternations can still be distinguished. The more diatomaceous green deposits are interpreted as interglacial stages. Samples analyzed for TEX_{86} were chosen from all the different lithologies (Fig. 2). In particular the (diatomaceous) laminated and bioturbated deposits were sampled, so we can test whether the glacial-interglacial variability inferred from the lithology is reflected in our TEX_{86} data.

2.3 Oligocene and Miocene paleoceanographic setting

The Oligocene and Miocene Southern Ocean paleoceanographic configuration is still obscure and controversial. Some studies suggest that most Southern Ocean surface and deep water masses were already in place by Eocene-Oligocene boundary times (Katz et al., 2011). Neodymium isotopes on opposite sides of Tasmania suggest that an eastward flowing deep-water current was present since 30 Ma (Scher et al., 2015). A westward flowing Antarctic Circumpolar Counter Current (ACCC) was already established during the middle Eocene (49 Ma; Bijl et al. 2013) (Fig. 1). Tasmanian gateway opening also allowed the proto-Leeuwin current (PLC) flowing along southern Australia continue eastward (Carter et al., 2004; Stickley et al., 2004) (Fig. 1). However, numerical modeling studies show that throughflow of the Antarctic Circumpolar Current (ACC) was still limited during the Oligocene (Hill et al., 2013), because Australia and South America were substantially closer to Antarctica (Fig. 1) than today (Markwick 2007). Moreover, tectonic reconstructions and stratigraphy of formations on Tierra del Fuego suggest that following open conditions in the middle and late Eocene, the seaways at Drake Passage underwent uplift starting at 29 Ma and definitive closure around 22 Ma (Lagabrielle et al., 2009). Evidence for active spreading and transgressional deposits in the Tierra del Fuego area record the widening of Drake Passage from 15 Ma onwards. The timing of the Drake Passage opening, which allowed for significant ACC throughflow, is still heavily debated (Lawver & Gahagan 2003; Livermore et al., 2004; Scher & Martin 2006; 2008; Barker et al., 2007; Maldonado et al., 2014; Dalziel 2014). Contourite deposits suggest that strong Antarctic bottom water currents first appeared in the early Miocene (21.3 Ma) and that Weddell Sea Deep Water was able to flow westwards into the Scotia Basin since the middle Miocene (~12.1 Ma) (Maldonado et al., 2003; 2005). It has been suggested that the closure and the reopening of Drake Passage are responsible for the warmer late Oligocene and the Miocene Climatic Optimum (MCO), and the subsequent cooling during the Miocene Climate Transition (MCT), respectively, as inferred from the benthic $\delta^{18}O$ records (Lagabrielle et al., 2009). If the throughflow at the Drake Passage was limited in the late Oligocene and early Miocene, the Antarctic Circumpolar Counter Current (ACCC) was more dominant than the ACC during these times according to the model study of Hill et al. (2013).

Antarctica was positioned more eastward during the Oligocene and Miocene relative to today (due to true polar wander; van Hinsbergen et al., 2015), and Site U1356 was more to the north during the Oligocene and Miocene compared to today (58.5°S at 34 Ma to 61.2°S at 10 Ma). Reconstructions of the position of the PF based on the

distribution of calcareous and siliceous microfossils, place the PF at 60°S during the early Oligocene (Scher et al., 2015), which means that Site U1356 may have crossed the PF between 34 and 10 Ma. The more northerly position of Site U1356 may have facilitated the influence of warmer waters during the mid-Miocene at Site U1356 (Sangiorgi et al., 2018), and therefore bottom-water formation may have been absent or limited at Site U1356. Bottom-water formation is expected in more southerly positioned shallow basins where glaciers extended onto the Antarctic shelf, such as the nearby Ross Sea (Sorlien et al., 2007). However, neodymium isotopes obtained from Site U1356 suggest that bottom water formed offshore the Adélie and Wilkes Land coast during the Early Eocene, which seems in contrast with the globally high temperature of that time (Huck et al., 2017). Modeling studies have, however, suggested that density contrasts created by seasonal changes in SST and salinity (with or without sea ice) may have induced deep-water formation and downwelling around Antarctica (Goldner et al., 2014; Lunt et al., 2010).

2.4 Age model U1356

Oligocene sediments were recovered in the section from 894.68 mbsf (first occurrence (FO) *Malvinia escutiana*) to 432.64 mbsf (base of subchron C6Cn.2n) at IODP Hole U1356A (Bijl et al., 2018). The shipboard age model (Tauxe et al., 2012) was based on biostratigraphy with magnetostratigraphic tie points and chronostratigraphically calibrated to the Geologic Timescale of 2004 (Gradstein et al., 2004). We follow Bijl et al. (2018), who recalibrated the existing age tie points to the Geologic Timescale of 2012 (GTS2012, Gradstein et al., 2012). The FO of *Malvinia escutiana* (894.68 mbsf; 33.5 Ma; Houben et al., 2011) and the last occurrence (LO) of *Reticulofenestra bisecta* (431.99 mbsf; 22.97 Ma) and the paleomagnetic tie points were used to convert the data to the time domain (see Fig. 4). For the Oligocene-Miocene Boundary, we also follow Bijl et al. (2018) who infer a hiatus spanning ~22.5-17.0 Ma between Cores 44R and 45R (~421 mbsf). It is unknown whether additional short hiatuses exist within the Oligocene record, but this is likely considering the presence of MTDs (Salabarnada et al., submitted this volume; Fig. S1). In addition, the poor core recovery in some intervals dictates caution in making detailed stratigraphic comparisons with other records.

For the Miocene section of Hole U1356A we follow Sangiorgi et al. (2018), who applied the Constrained Optimization methodology (CONOP) of Crampton et al. (2016) on diatom and radiolarian biostratigraphic events to construct an age model. Based on the application of CONOP to the diatom and radiolarian biostratigraphic events a second hiatus was identified spanning approximately the interval between 13.4 and 11 Ma.

2.5 Glycerol dialkyl glycerol tetraether extraction and analysis

In addition to the 29 samples from the Miocene section presented in Sangiorgi et al. (2018), a total of 132 samples from the Oligocene and early Miocene part of the sedimentary record (Table S1) were processed for the analysis of glycerol dialkyl glycerol tetraethers (GDGTs) used for TEX_{86}. Spacing varies due to variability in core recovery and GDGT preservation. Furthermore, sampling of contorted strata was avoided. Sample processing involved manual powdering of freeze-dried sediments after which lipids were extracted through accelerated solvent extraction (ASE;

with dichloromethane (DCM)/methanol (MeOH) mixture, 9:1 v/v, at 100°C and 7.6 x 10^6 Pa). The lipid extract was separated using Al_2O_3 column chromatography and hexane/DCM (9:1, v/v), hexane/DCM (1:1, v/v) and DCM/MeOH (1:1, v/v) for separating apolar, ketone and polar fractions, respectively. Then, 99 ng of C_{46} internal standard was added to the polar fraction, containing the GDGTs, for quantification purposes (cf. Huguet et al.,

230   2006). The polar fraction of each sample was dried under N_2, dissolved in hexane/isopropanol (99:1, v/v) and filtered through a 0.45-µm 4-mm-diameter polytetrafluorethylene filter. After that the dissolved polar fractions were injected and analyzed by high performance liquid chromatography/mass spectrometry (HPLC/MS) at Utrecht University. Most samples were analyzed following HPLC/MS settings in Schouten et al. (2007), while some samples (see Table S1) were analyzed by ultra-high performance liquid chromatography/mass spectrometry

235   (UHPLC/MS) according to the method described by Hopmans et al., (2016). Only a minor difference between TEX_{86} index values generated by the different methods was recorded by Hopmans et al. (2016) (on average 0.005 TEX_{86} units). Reruns of 5 samples with the new method show an average difference between the two methods of 0.011 TEX_{86} units (see Table S2), which translates to a 0.6°C temperature difference based on TEX_{86}^H of Kim et al., (2010) and lies well within the calibration error of 2.5°C. GDGT peaks in the (U)HPLC chromatograms were

240   integrated using Chemstation software. Sixteen of the 132 samples had too low concentrations of GDGTs to obtain a reliable TEX_{86} value and have been discarded.

We have used the branched and isoprenoid tetraether (BIT) index (Hopmans et al., 2004) to verify the relative contribution of terrestrial GDGTs in our samples, compared to marine GDGTs. As isoprenoid GDGTs (isoGDGTs), used for the TEX_{86} proxy are also produced in terrestrial soils, albeit in minor amounts, they can alter the marine

245   signal when there is a large contribution of soil organic matter to marine sediments. This contribution can be identified by determining the relative amount of branched GDGTs (brGDGTs), which are primarily soil-derived (Weijers et al., 2006), to that of the isoGDGT crenarchaeol (Hopmans et al., 2004). Samples with BIT index values above 0.3 indicate that the TEX_{86}-based temperature may be affected by a contribution of soil-derived isoGDGTs and thus should be discarded (cf. Weijers et al. 2006), although, a high BIT value can sometimes also result from

250   production of brGDGTs in marine sediments and the water column (Peterse et al., 2009; Sinninghe Damsté, 2016). The composition of the brGDGTs can be used to distinguish between marine and soil-derived GDGT input, in particular by using the #ring$_{tetra}$ index (Sinninghe Damsté, 2016). The #rings$_{tetra}$ index can discriminate between marine and soil-derived brGDGTs as the composition of soil-derived GDGTs typically show high amounts of the acyclic tetramethylated GDGT-Ia, while a dominance of cyclic tetramethylated (Ib and Ic) brGDGTs has been

255   attributed to *in situ* production within the sediments (Sinninghe Damsté, 2016).

Oxic degradation of GDGTs does not affect the relative amounts of individual isoGDGTs (Huguet et al., 2009; Kim et al., 2009). However, oxic degradation may lead to an increased relative influence of soil-derived isoGDGTs, which could bias the TEX_{86} in different ways depending on the composition of the soil-derived isoGDGTs (Huguet et al., 2009). Enhanced BIT index values are expected in samples with enhanced amounts of soil-derived isoGDGTs

260   due to oxic degradation, and will be discarded. In addition, we calculated the Methane Index (MI) (Zhang et al., 2011), GDGT-0/crenarchaeol (Blaga et al., 2009; Sinninghe Damste et al., 2009), GDGT-2/crenarchaeol ratios

(Weijers et al., 2011), and Ring Index (Zhang et al., 2016) to check for input of methanogenic or methanotrophic archaea, or any other non-temperature related biases to TEX_{86}.

2.6 TEX_{86} calibrations

265 The TEX_{86} proxy is based on the distribution of isoGDGTs preserved in sediments (Schouten et al., 2013, 2002). In marine sediments these lipids are assumed to originate from cell membranes of marine Thaumarchaeota, which are one of the dominant prokaryotes in today's ocean and occur throughout the entire water column (e.g. Karner et al. 2001; Church et al. 2010, 2003). Applying TEX_{86} in polar oceans has been challenged by the observation that high scatter in the cold end of the core top dataset for TEX_{86} is present (Ho et al., 2014; Kim et al., 2010). To overcome

270 some of the scatter as well as the non-linearity of the TEX_{86}-SST relationship, Kim et al. (2010) proposed two isoGDGT-based proxies and calibrations: TEX_{86}^{L} and TEX_{86}^{H}. The latter is not considered here as it was particularly developed for low-latitude high-temperature surface waters, and high-latitude core-top values were left out of the calibration (Kim et al., 2010). The former was particularly developed for high-latitude low-temperature surface waters. However, it has been shown that TEX_{86}^{L} is sensitive to changes in the GDGT-2/GDGT-3 ratio ([2]/[3]),

275 which are unrelated to SST (Taylor et al., 2013; Hernández-Sánchez et al., 2014). Instead these [2]/[3] changes result from changes in the Thaumarchaeotal community structure in the water column, because the community that thrives in deeper (>1000 mbsl) nutrient and ammonia-rich waters, produces significantly more GDGT-2 and thereby introduces a water-depth dependency into the calibration (Taylor et al., 2013; Hernández-Sánchez et al., 2014; Villanueva et al., 2015). Close to the Antarctic margin, the abundance of 'shallow' versus 'deep water'

280 Thaumarchaeotal communities at deep-water sites, like Site U1356 during the Oligocene-Miocene, could be affected by the presence of sea ice and the relative influence of (proto-)UCDW and (proto-)LCDW upwelling. For this reason, also TEX_{86}^{L}-based calibrations are not the focus of our study. Instead, we focus on TEX_{86}-based calibrations only. All existing $TEX_{86}^{(H)}$ and TEX_{86}^{L} calibrations have, however, been applied to our data and are presented as a supplementary figure (Figure S1).

285 The latest global calibration set that includes also the high-latitude core-top values is the linear SST calibration of Kim et al. (2010). Despite the scatter at the cold end of the calibration that results from the inclusion of Arctic surface sediment samples with deviating TEX_{86}-SST relations, this calibration (SST = 81.5*TEX_{86} – 26.6 with a calibration error of ±5.2°C) has been shown to plot onto the annual mean sea surface temperatures of the World Ocean Atlas 2009 (WOA2009; Locarnini et al. 2010) for the surface-sample TEX_{86} values obtained in the Pacific

290 sector of the Southern Ocean (Ho et al., 2014). However, this calibration is likely to be influenced by regional differences in water depth, oceanographic setting and archaeal communities (Kim et al., 2015; 2016; Tierney and Tingley, 2014; Trommer et al., 2009; Villanueva et al., 2015). In addition, this calibration suffers from regression dilution bias caused by the uncertainty in the measured TEX_{86} values plotted on the x-axis (Tierney & Tingley 2014). Regression dilution bias causes flattening of the slope (Hutcheon et al., 2010) and therefore affects

295 reconstructed TEX_{86}-based temperatures at the lower and upper end of the calibration range. Modern-analogue calibration methods exist today to overcome this regression dilution bias as well as some of the regional variability of TEX_{86}-SST relationships (Tierney and Tingley, 2015, 2014). These calibrations are based on a Bayesian spatially

varying regression model (BAYSPAR), which infers a best estimate for intersection and slope of the calibration based on an assembly of 20° by 20° spatial grid boxes that statistically fit best with an estimate of the prior

300   distribution of temperature (i.e. the prior) (Tierney and Tingley, 2014). As for deep-time temperature reconstructions this prior cannot be based on modern-day annual mean sea surface temperatures, the BAYSPAR method requires a user-specified mean and variance for this prior (Tierney and Tingley, 2014). The prior for Site U1356 is obtained from recent clumped isotope measurements (Δ_{47}) on planktonic foraminifers from Maud Rise (ODP Site 689) (Petersen and Schrag, 2015), which show early Oligocene temperatures of 12°C. The BAYSPAR approach (Tierney

305   & Tingley 2014; 2015) selects only those TEX_{86} values from the calibration set of Kim et al. (2010) and an additional 155 core-tops from regional core-top TEX_{86} studies, that are relevant for the study site, thereby generating a more regional calibration. Application of BAYSPAR on Site U1356 using a prior mean of 12°C does, however, result in the exclusion of the high-latitude core-top values. For this reason we find it useful to compare the BAYSPAR results to the results obtained by using the linear calibration of Kim et al. (2010). The BAYSPAR

310   calibration method provides an estimate for SST and an upper and lower 90% confidence interval. For comparison to the linear calibration of Kim et al. (2010) a standard error (SE) has been calculated from these confidence intervals by assuming a normal distribution around the mean, in which case the 90% confidence interval boundaries can be calculated as the mean plus or minus 1.645 times SE.

Despite these recent efforts in improving the TEX_{86}-SST relationship, TEX_{86} is known to overestimate temperatures

315   at high latitudes due to multiple possible biases, such as seasonality (Ho et al., 2014; Schouten et al., 2013) and the incorporation of a subsurface signal (0-200 mbsl) at deep-ocean sites (>1000 mbsl) (Hernández-Sánchez et al, 2014; Huguet et al. 2007; Rodrigo-Gámiz et al., 2015; Yamamoto et al., 2012). There is, however, general consensus that TEX_{86} is able to capture decadal and longer-term temperature trends (Richey and Tierney, 2016), which is why the main focus of this work is on relative SST changes. Indeed, subsurface export of GDGTs is implicitly incorporated

320   into the global TEX_{86}-SST calibration and has therefore no implications for reconstructing SST (Hernández-Sánchez et al., 2014). Highest GDGT fluxes are closely linked to highest organic matter, opal (diatom frustules) and lithogenic particle fluxes (Mollenhauer et al., 2015; Yamamoto et al., 2012) and the lack of production of sinking particles that can incorporate GDGTs formed in deeper waters prevents biasing of surface-sediment TEX_{86} values towards deep-water temperatures (Basse et al., 2014; Mollenhauer et al., 2015; Yamamoto et al., 2012). Still,

325   particular environmental settings (e.g., upwelling regions, regions with oxygen-depleted deep waters, fresh-water surface waters) might favor the transport of a subsurface temperature (subT) signal to the sediments (Kim et al., 2012a, 2012b; Lopes dos Santos et al., 2010; Mollenhauer et al., 2015). Also for polar oceans it has been suggested that reconstructed temperatures reflect subT, since today Thaumarchaeota are virtually absent in the upper 0-45 m of Antarctic low-salinity surface waters formed by seasonal retreat of sea ice (Kalanetra et al., 2009). Surface water

330   conditions over Site U1356 during the Oligocene and the MCO were much like present-day regions south of the Subtropical Front (STF) and likely not under the influence of a seasonal sea ice system (see Fig. 1) (Sangiorgi et al., 2018; Bijl et al., submitted this volume). For these time intervals, there is no reason to believe that surface waters were devoid of Thaumarchaeota due to the presence of sea ice and that TEX_{86} values are influenced by an increased subsurface signal. For the earliest Oligocene and the MCT, the presence of *Selenopemphix antarctica* suggests that

335   Site U1356 was under the influence of a seasonal sea-ice system (Bijl et al., submitted this volume). For these

periods, a reconstruction of subT values may be more appropriate, but this would still imply that SSTs are warmer.

We limit our discussion to the TEX$_{86}$-based reconstructions to SST, notably, because it has been shown that TEX$_{86}$-

based SST estimates based on the linear calibration of Kim et al. (2010) obtained from core-top samples from

today's sea ice-influenced Southern Ocean, are in accordance with WOA2009 mean annual SST (Ho et al., 2014).

340   This suggests that the effect of sea ice on surface and subsurface isoGDGT production is incorporated into the linear

calibration of Kim et al. (2010). We therefore consider that despite the potential absence of Thaumarchaeota in the

surface waters during the early Oligocene and the MCT, the calibration of Kim et al. (2010) does provide a reliable

estimate of SST for these time intervals. Moreover, [2]/[3] ratios for the earliest Oligocene and the MCT are

relatively low and show much less variability compared to the rest of the record (Fig. 2), which is opposite to what is

345   expected when the relative influence of deep-water Thaumarchaeota increases (Hernández-Sánchez et al., 2014;

Villanueva et al., 2015). Calibrations to subT (Kim et al., 2012a; Kim et al., 2012b; Tierney & Tingley, 2015) are

therefore not considered here, but are included in supplementary Figure S1.

To get an estimate for the long-term average SST trends and confidence levels a Local polynomial regression model

(LOESS) has been applied using R, which is based on the local regression model *cloess* of Cleveland et al. (1992).

350   This method of estimating the long-term average trend is preferred over a running average, because it accounts for

the variable sample resolution. For the parameter *span*, which controls the degree of smoothing a value was

automatically selected through generalized cross-validation (R-package fANCOVA; Wang 2010).

3 Results

3.1 Discarding potentially biased TEX$_{86}$ values

355   A total of 113 samples spanning the Oligocene were analyzed for TEX$_{86}$ in this study. When the Miocene samples

of Sangiorgi et al. (2018) are included, the total number of samples with sufficiently high GDGT concentrations is

145. However, only 77 of these 145 TEX$_{86}$ values could be used for SST reconstruction for reasons discussed below.

Although sampling of contorted strata was avoided, a total number of 46 Oligocene and Miocene samples proved to

be obtained from MTDs after detailed logging by Salabarnada et al. (submitted this volume). Hence, samples from

360   these beds may not reflect *in situ* material exclusively. For the EOT slumps, this is supported by a high degree of

reworked Eocene specimens within the dinoflagellate cyst assemblage below 880.08 mbsf (Houben et al., 2013). In

addition, the clast-bearing deposits of Unit II and IV and decimeter-thick granule-rich interbeds of Unit VIII (Fig. 2)

are interpreted as ice-rafted debris (IRD) deposits (Escutia et al., 2011; Sangiorgi et al., 2018), and thus indicate the

presence of icebergs above the site during deposition of these intervals. To avoid potential bias due to allochtonous

365   input and reworking of older sediments, all samples from MTDs are excluded from the SST reconstructions.

A contribution of terrestrial isoGDGTs can also bias the marine pelagic TEX$_{86}$ signal, and can be verified by the

BIT index (Hopmans et al., 2004; Weijers et al., 2006). In seventeen samples – none of which were derived from

MTDs – the BIT index value was >0.3, which indicates that the reconstructed TEX$_{86}$ temperatures are likely affected

by a contribution of soil-derived isoGDGTs (Weijers et al., 2006; Hopmans et al. 2004). For selected samples, the

370   composition of brGDGTs was analyzed by UHPLC/MS (Hopmans et al., 2016), which showed that #rings$_{tetra}$ were above 0.7 (Sinninghe Damsté, 2016) meaning that a significant portion of the brGDGTs was likely soil-derived. Furthermore, the TEX$_{86}$ signal may be influenced by a potential input of isoGDGTs from methanogenic archaea. Since methanogenic Euryarchaeota are known to produce GDGT-0 (Koga et al., 1998), but not crenarchaeol such a contribution may be recognized by GDGT-0/crenarchaeol values >2 (Blaga et al., 2009; Sinninghe Damsté et al.,

375   2009). Similarly, methanotrophic Euryarchaeota may contribute significant amounts of GDGT-1, GDGT-2 and GDGT-3that can be identified by values >0.3 for the Methane Index (MI) (Zhang et al., 2011) and/or GDGT-2/crenarchaeol values >0.4 (Weijers et al., 2011). In total nineteen non-MTD-derived samples have too high GDGT-0/crenarchaeol ratios, too high Methane Index values, or too high GDGT-2/crenarchaeol values. Fourteen of these nineteen samples also have too high BIT values, meaning that in total 22 samples are discarded because of a

380   potential contribution of soil-derived and methanogenic or methanotrophic archaeal isoGDGT input. As a final exercise, the Ring Index ($|\Delta RI|$) was calculated for our dataset to identify all other non-temperature related influences on the distribution of isoGDGTs in the samples (Zhang et al., 2016). In addition to the non-temperature related influences discussed above, these could include oxygen concentrations (Qin et al., 2015), archaeal growth phase (Elling et al., 2014), ammonia oxidation rates (Hurley et al., 2016) and ecological factors (Elling et al., 2015).

385   Using $|\Delta RI|>0.6$ as a cutoff, no additional samples were discarded. All GDGT data and TEX$_{86}$ values, including that of the discarded samples, are presented in the supplementary material (Figure S2, Table S1).

3.2 Relation between TEX$_{86}$ values and lithology

After excluding samples with potentially biased TEX$_{86}$ values, the remaining record shows short-term variability that is strongly linked to the lithology (see Fig. 2). Sediments from the greenish laminated, carbonate-poor (glacial)

390   facies produce statistically significant (t-test p-value < 0.005) lower TEX$_{86}$ values than values obtained from the grey carbonate-rich bioturbated (interglacial) facies. For the entire record, TEX$_{86}$ values are on average 0.50 and 0.53 for the glacial (laminated) and interglacial (bioturbated) lithologies, respectively. Paleoceanographic changes between glacial and interglacial periods may have affected the community structure of the Thaumarchaeota living over Site U1356, which may have introduced a non-thermal component to the TEX$_{86}$ record that could contribute to

395   the observed difference between TEX$_{86}$ values from laminated and bioturbated facies. To test if changes in the composition of the Thaumarchaeotal community have contributed significantly to the observed difference between TEX$_{86}$ values from laminated facies and bioturbated facies, a t-test was also performed on the [2]/[3] ratios of laminated and bioturbated lithologies for the entire record (Fig. 2). No significant difference was observed between the laminated and bioturbated facies (t-test p-value > 0.2).

400   ### 3.3 Oligocene and Miocene long-term sea surface temperature trend

Based on the linear temperature calibration of Kim et al. (2010) (black curve in Fig. 3A), our TEX$_{86}$ values yield highest temperatures around 30.5 Ma (up to 22.6±5.2°C), 25.5 Ma (up to 25.1°C±5.2°C) and around 17 Ma (up to 19.2±5.2°C), whereas lowest temperatures are recorded between 22 and 23.5 Ma (minimum temperatures are

8.3°C±5.2°C), and around 13 and 10.5 Ma (minima around 7.6±5.2°C). On average SSTs based on the linear calibration of Kim et al. (2010) are 16.6°C, 16.7°C and 10.6°C for the Oligocene, MCO and MCT, respectively. Oligocene SST variability increases significantly (p-value<0.001 in F-test) after 26.5 Ma (see Fig. 3B). Before 26.5 Ma, the variation in the record (2σ) is of 3.6°C, while the 2σ is 6.8°C after 26.5 Ma. We note a strong (9.5°C) SST drop at the lower boundary of what is interpreted to represent subchron C6Cn.2n (23.03 Ma) (see Fig. 2 and 4); at the stratigraphic position of maximum $\delta^{18}O$ values related to Mi-1 in the deep-sea records (Beddow et al., 2016; Liebrand et al., 2011; Pälike et al., 2006b). Unfortunately, due to core recovery issues, limited high-resolution chronobiostratigraphic control in this interval, the age model generally lacks the resolution to identify some of the other known transient temperature drops in our record (~30 Ma, ~24 Ma) to Oligocene glaciation-related Oi-events (Fig. 4).

The SST record for Site U1356 based on the BAYSPAR model shows the same trend as the SST record generated with the linear calibration, but for SST values below 20.5°C it is offset towards slightly warmer values for SSTs based on the linear calibration below 20.5°C. Above 20.5°C, BAYSPAR-based SSTs are slightly offset towards cooler values. On average the BAYSPAR-based SSTs are 0.8°C warmer than the SSTs based on the linear calibration of Kim et al. (2010), and they have a smaller calibration SE (±4.0°C) (red curve in Fig. 3A). This offset and the smaller calibration error result primarily from the fact that BAYSPAR-calibration does not take the polar TEX_{86} core-top values into account. Instead, it bases its calibration mostly on the modern 30-50° northern and southern latitudinal bands (see map in Fig. 3). Nevertheless, the BAYSPAR-based SSTs lie well within the ±5.2°C SE of the transfer function from Kim et al. (2010), as well as within the SE of about ±4.0°C for the BAYSPAR SST calibration. Average SSTs for the Oligocene, MCO and MCT based on the BAYSPAR SST calibration are 17.2°C, 17.3°C and 12°C, respectively.

4 Discussion

4.1 Oligocene and Miocene Southern Ocean sea surface temperatures

Our TEX_{86}-derived SST record is the first for the Southern Ocean that covers almost the entire Oligocene. Absolute temperature values are relatively high considering the high-latitude position of Site U1356 (~59°S, van Hinsbergen et al., 2015), but confidence can be obtained from the observation that TEX_{86}-based reconstructed SSTs from glacial lithologies are generally lower than those from interglacial lithologies (Fig. 4). Several lines of evidence support the relatively high Oligocene and mid-Miocene temperatures reconstructed for Site U1356. Dinoflagellate cyst assemblages from the same site (Sangiorgi et al., 2018; Bijl et al., submitted this volume) mostly contain taxa related to those found between the Polar (PF) and the Subtropical Front (STF) today, where mean annual sea surface temperature is between 8 and 16°C (Prebble et al. 2013). This is on the low end of our reconstructed SSTs for the Oligocene and the MCO, but very comparable to SSTs for the MCT. Furthermore, the abundance of *in situ* pollen of temperate vegetation in these sediments (Sangiorgi et al., 2018; Strother et al., 2017), which are most likely derived from the Antarctic shores, also suggests a relatively mild climate. Finally, the abundance of pelagic carbonaceous

facies in some of the Oligocene interglacial intervals of these high-latitude strata is interpreted to occur under the influence of warmer northern-sourced surface waters at Site U1356 (Salabarnada et al., submitted this volume).

440   In general, Oligocene SST estimates are higher than the SST estimates reconstructed with other proxies in other high-latitude Southern-Ocean Sites 511 and 689 (Fig. 3A). However, the reconstructed ~12°C (standard error: ±1.1-3.5°C) based on clumped isotopes from Site 689 is derived from thermocline-dwelling foraminifera, whereas the temperature of the surface waters was likely higher than that at the thermocline (Petersen and Schrag, 2015). In addition, when the newest calibration for clumped isotope data is applied (Kelson et al., 2017) also higher

445   temperature estimates, 12.8-14.5°C, are obtained. Temperature estimates between 6 and 10°C have been obtained from ODP Site 511 (see Fig. 1) based on $U^{K'}_{37}$ (Plancq et al., 2014) and TEX_{86} values (Liu et al., 2009), the latter recalculated with the linear calibration of Kim et al. (2010) and the BAYSPAR calibration used here (Fig. 3A). The influence of the cold Antarctic-derived surface current at Site 511 (Bijl et al., 2011; Douglas et al., 2014) (Fig. 1) might be the reason of these colder estimates. Similar to the Eocene, Site U1356 probably was one of the warmest

450   regions around Antarctica during the early Oligocene (Pross et al., 2012), situated at a relatively northerly latitude (van Hinsbergen et al., 2015) and still under influence of relatively warm proto-Leeuwin current (PLC, Fig. 1) (Bijl et al. 2011; submitted this volume).
Sangiorgi et al. (2018) compared TEX_{86}^{L}-based reconstructed temperatures (based on the 0-200 depth-integrated calibration of Kim et al., 2012a) from the Miocene section of Site U1356 with Mg/Ca-based SST values from

455   planktic foraminifera from ODP Site 1171, South Tasman Rise (Shevenell et al., 2004), and TEX_{86}^{L}-based seawater temperatures from the ANDRILL (AND)-2A core, Ross Sea (Levy et al., 2016). Based on these temperature reconstructions it was established that temperatures at Site U1356 during the MCO are very comparable to the Mg/Ca-based SSTs from the South Tasman Rise are and a few degrees cooler during the MCT, which was further supported by pollen and dinocyst assemblages (Sangiorgi et al., 2018). We reach the same conclusion based on the

460   reconstructed SSTs using the linear calibration of Kim et al. (2010) and the BAYSPAR calibration for the Miocene TEX_{86} values from Site U1356 as well as site AND-2A (Fig. 3). Based on these recalibrated SST values, we conclude, like Sangiorgi et al. (2018), that there was a much reduced SST gradient between Site U1356A and Site 1171, which were at that time positioned at approximately 60.0°S and 53.6°S, respectively (van Hinsbergen et al., 2015). Notably, however, the latitudinal difference between the Site U1356 and Site 1171 increased as well and may

465   be partly responsible for the increased temperature gradient between the two sites at 14 Ma (Site U1356 lay at 60.5°S and Site 1171 lay at 52.7°S; van Hinsbergen et al., 2015).
Biota-based temperature reconstructions at such high latitudes are likely skewed towards summer conditions, as has also been suggested for Site 689 and Site 511 (Petersen and Schrag, 2015; Plancq et al., 2014). An important reason for this could be the light limitation at high latitudes during winter (e.g., Spilling et al. 2015), which is unfavorable

470   for the growth and bloom of phytoplankton, and organisms feeding on phytoplankton. The potential summer bias in high latitude TEX_{86}-based SST reconstructions has been discussed extensively for other past warm periods (e.g., Sluijs et al., 2008; Bijl et al., 2009; 2010; 2013). Like in these past warm climates, we expect that primary productivity in the Oligocene Southern Ocean was in sync with seasonal availability of light, irrespective of the presence of sea ice or overall climate conditions. Indeed, isoGDGTs likely require pelleting to sink effectively

475   through the water column to the ocean floor (e.g., Schouten et al. 2013), and therefore depend on the presence of larger zooplankton that feed on the phytoplankton. As phytoplankton blooms mostly occur during Antarctic summer/autumn, as do their predators (Schnack-Schiel, 2001), we expect the highest isoGDGT fluxes to the sediment during the summer in the Southern Ocean, despite their highest production during a different season (Church et al., 2003; Murray et al., 1998; Richey and Tierney, 2016; Rodrigo-Gámiz et al., 2015). A bias towards

480   summer temperatures is confirmed by the presence of sea-ice dinoflagellate cysts in some parts of the record, which would suggest SSTs near freezing point during winter.

4.2 Long-term Oligocene and Miocene sea surface temperature trends

We aim to explore the implications of the long-term trends in our TEX$_{86}$-based SST record, by placing it in context of the global benthic δ^{18}O and benthic foraminiferal Mg/Ca-based bottom-water temperature (BWT) records, in

485   order to infer oceanographic changes or changes in ice volume. Due to the relatively low sample resolution, and discontinuous sampling due to core gaps, in comparison to the complete and quasi-continuous δ^{18}O records (Beddow et al., 2016; Billups et al. 2004; Hauptvogel et al., 2017; Holbourn et al., 2015; Liebrand et al., 2017, 2016; Pälike et al., 2006a; 2006b), we will here focus on the long-term temperature trends. However, we can use the glacial-interglacial alternations in the lithology, which cover the period between 32 and 10 Ma, to differentiate

490   between glacial and interglacial SST and assess amplitudes (see Fig. 2). As was mentioned, SSTs derived from the glacial facies show a significantly lower mean than SSTs derived from interglacial facies. Separating glacial and interglacial signals allows us to interpret the long-term SST trend, as this removes a potential sampling bias caused by irregularly spaced glacial or more interglacial samples. To obtain both long-term glacial and interglacial SST trends, LOESS curves are plotted through SST estimates from the glacial and interglacial subsets of the Oligocene

495   (Fig. 4). For the Miocene we averaged SSTs from glacial and interglacial samples for the three-sample 'cluster' (at ~17, ~13.5 and ~10.5 Ma). Glacial and interglacial LOESS curves plotted through the SST estimates based on the linear calibration of Kim et al. (2010) show the same trend, lying slightly below the BAYSPAR SST LOESS curves (Fig. 4).

A global benthic foraminiferal stacked δ^{18}O curve has been constructed by combining the benthic δ^{18}O records of

500   the far-field Site 1218, eastern equatorial Pacific (Pälike et al., 2006b); Sites 1264/1265, Walvis Ridge, southeast Atlantic (Liebrand et al., 2017, 2016); Sites 926/929, Ceara Rise, equatorial Atlantic (Pälike et al., 2006a ; Zachos et al., 2001); Site U1334, eastern equatorial Pacific (Beddow et al., 2016); Site 1090, Agulhas Ridge, Atlantic sector of the Southern Ocean (Billups et al., 2004); Site U1337, eastern equatorial Pacific (Holbourn et al., 2015); and Site 588, southwest Pacific (Flower & Kennett, 1993). To obtain a global benthic δ^{18}O stack in which the global long-

505   term trends are best represented, we have normalized the data to the Site 1264/1265 record of Liebrand et al. (2017, 2016), on which all records now overlap (Fig.4). Mg/Ca-based BWT records are obtained from Site 1218, eastern equatorial Pacific (Lear et al., 2004); Site 747, Kerguelen Plateau, Southern Ocean (Billups & Schrag, 2002); and Site 1171, Tasman Rise, Southern Ocean (Shevenell et al., 2004). LOESS curves have been plotted through the benthic δ^{18}O stack as well as the individual Mg/Ca-based BWT records (Fig. 4).

510   The LOESS curves through the glacial and interglacial data show similar trends and show a striking resemblance to the global benthic δ^{18}O stack (Fig. 4), particularly when considering the compromised sample resolution of our record. The temperature optima and minima in the LOESS curves can be directly linked to periods of relatively low and high benthic δ^{18}O values (maximum and minimum ice volume/BWT), respectively. Temperatures increase from the earliest Oligocene towards 30.5 Ma, while benthic δ^{18}O values show a decrease in the same interval, but reach a

515   minimum earlier, around 32 Ma. It is difficult to determine whether SSTs are truly lagging the benthic δ^{18}O values in this interval or whether this is an artifact caused by the age model in this part of the record. The recorded post-Oi-1 SST warming coincides with the disappearance of IRD (Escutia et al., 2011) and sea-ice related dinoflagellate cysts (Houben et al., 2013) in the same record (Fig. 4). Following this temperature optimum, there is a cooling trend until a minimum is reached around 28-27 Ma, which coincides with relatively high benthic δ^{18}O values and the Oi-

520   2a and Oi-2b glacials. Subsequently, there is a warming towards a long-term temperature optimum around 25 Ma, which coincides with a minimum in the benthic δ^{18}O record known as the late Oligocene warming. This temperature optimum around 25 Ma is characterized by the influx of the temperate dinocyst species *Nematosphaeropsis labyrinthus* (Bijl et al., submitted this volume). This seems to indicate a strong influence of northern-sourced surface waters at Site U1356, as this species is currently associated with the Subtropical Front and winter and summer

525   temperatures of 6–13°C and 8–17°C, respectively (Esper and Zonneveld, 2007; Marret and De Vernal, 1997; Prebble et al., 2013). Finally, the Oligocene LOESS temperature curves show a cooling towards the Oligocene-Miocene transition at 23 Ma. In comparison to the benthic δ^{18}O record this cooling trend is rather gradual and starts 1 Myr earlier than the steeper benthic δ^{18}O record increase that starts at 24 Ma and continuous towards the Mi-1 glaciation. We consider this to represent a realistic climate signal, notably so since the age model is sufficiently

530   well-constrained in this part of the record. Glacial and interglacial averages for the Miocene data clustered around 17, 13.5 and 10.5 Ma show a declining trend and follow the increasing benthic δ^{18}O trend that characterizes the MCT. High amounts of *N. labyrinthus* within the MCO interval support warm surface water conditions (Sangiorgi et al., 2018). After the MCO, increased amounts of sea-ice dinoflagellates and IRD indicate that Site U1356 came under the influence of seasonal sea ice, and therefore cooler conditions. However, increases of *N. labyrinthus* after

535   the MCT indicate that warmer northern-sourced waters still periodically influenced Site U1356 (Sangiorgi et al., 2018).

     The fact that the LOESS temperature trends mirror the benthic δ^{18}O record may suggest that (1) changes in the Wilkes Land SST correspond to SST changes in the region of deep-water formation, which is reflected in the benthic δ^{18}O records, (2) changes in the Wilkes Land SST reflect long-term changes in paleoceanography that

540   simultaneously affect or are related to the size of the Antarctic Ice Sheet (AIS) and therefore the deep-sea δ^{18}O of the sea water, or a combination of both.

     Considering the first, in the modern-day Southern Ocean, bottom water forms through mixing along the Antarctic Slope Front (ASF) of Circumpolar Deep Water (CDW) and High Salinity Shelf Water (HSSW), which forms in consequence of sea-ice formation (Gill, 1973; Jacobs, 1991). Associated with the ASF is the westward flowing

545   Antarctic Slope Current (ASC), which contributes to the bottom-water formation and results from the geostrophic adjustment of Ekman transport to the south, which is driven by the predominantly easterly winds around Antarctica

(Gill, 1973). It has been suggested that, after the establishment of its shallower westward flowing counterpart, the Antarctic Circumpolar Countercurrent (ACCC), around 49 Ma (Bijl et al., 2013), an ASC was established near Site U1356 in the early Oligocene (Scher et al., 2015). In areas where sea ice was formed during the Oligocene and

550 Miocene the ASC could have enhanced mixing between HSSW and CDW similarly to today. For the Wilkes Land margin this might have been the case for the earliest Oligocene and MCT where we find sea-ice indicators in the dinoflagellate cyst assemblages (Bijl et al., 2018; Houben et al., 2013). These sea-ice dinoflagellate cysts seem to indicate that winter temperatures at the Wilkes Land margin were cold enough to allow sea-ice formation and therefore maybe formation of deep waters along the Wilkes Land coast during the earliets Oligocene and MCT.

555 However, most of the record is devoid of sea-ice indicators, suggesting that modern-day process of deep-water formation, is unlikely to have occurred at the Wilkes Land Margin. Still, neodymium isotopes of fossil fish teeth from Site U1356 have suggested that deep-water formation took place at the Adélie and Wilkes Land Margin during the Eocene (Huck et al., 2017), when pollen indicate near-tropical warmth (Pross et al., 2012) . Model studies have suggested that during such warm periods seasonal density differences may still induce deep-water formation or

560 downwelling of waters around Antarctica (Goldner et al., 2014; Lunt et al., 2010). Alternatively and more likely, sea ice may have formed in the cooler Ross Sea and transported along the Wilkes Land coast similarly to today during the Oligocene and Miocene, meaning that deep water formed in the Ross Sea where glaciers extended onto the Antarctic shelf (cf. Sorlien et al., 2007). In that case, the absence of sea-ice dinoflagellate cysts during most of the Oligocene and the MCO at Site U1356 would mean that, in contrast to the earliest Oligocene and MCT, sea ice

565 coming from the Ross Sea was prevented from reaching Site U1356 by too warm winter SSTs. This is in accordance with the relatively warmer (summer) SST values for Site U1356 during most of the Oligocene and the MCO. If the reconstructed SST trends of Site U1356 are representative for the climatic trends of a larger region (i.e. including the Ross Sea as a potential region for deep water formation), this climatic signal may have been relayed to the deep ocean and recorded in the stable oxygen isotope composition of benthic foraminifera in far-field sites. In fact,

570 Southern Ocean-sourced deep waters may have reached as far as the north Pacific during the Oligocene (Borelli & Katz 2015). If this is the case, the consistent long-term trends between the SST of Site U1356 and the benthic $\delta^{18}O$ record would imply that the size of the AIS is less variable on these long-term timescales than the benthic $\delta^{18}O$ record would suggest under the assumption of constant BWT (e.g., Liebrand et al., 2017; see Figure 4): much of the variation will be due to deep-sea temperature variation. The small AIS may have been relatively stable during the

575 Oligocene and Miocene, most likely because there was less marine-based ice in comparison to land-based ice as topographic reconstructions of Antarctica would suggest (Gasson et al., 2016; Wilson et al., 2012).

Only one BWT record is available for the Oligocene, which is based on Mg/Ca ratios from Site 1218 (equatorial Pacific). Mg/Ca was obtained from the benthic foraminifer *Oridorsalis umbonatus* (Lear et al. 2004; Fig. 4), an infaunal species that is to some extent insulated from long-term changes in carbonate ion concentrations (Ford et al.,

580 2016; Lear et al., 2015). Although absolute temperatures may depend on local factors, such as pore water chemistry, the long-term trends should reflect the trends in BWT (Lear et al., 2015). The BWT record of Site 1218 shows a long-term deep-sea warming between 27 and 25 Ma, similar to our SST record. The temperature optimum at 30.5 Ma in our TEX_{86}-based SST record cannot be recognized in the BWT record of Site 1218. Similarly to the benthic

$\delta^{18}O$ record, an optimum is reached earlier (~32 Ma) and this mismatch could be due to uncertainties in the age

585 model of the lower part of the Oligocene section of Hole U1356A. The continued temperature rise after 25 Ma in the BWT record of Site 1218 is also not observed in our TEX_{86}-based temperature trend. This could be because the equatorial Pacific mainly receives bottom water from a warmer Pacific sector of the Southern Ocean, east of the Tasmanian Gateway, and not from the Wilkes Land margin, and the Pacific sector is influenced by warming. Alternatively, there is an increasing influence of a warmer deep-water mass from elsewhere. Notably, Mg/Ca-based

590 BWTs from Kerguelen Plateau (Site 747) show a temperature optimum around 25 Ma preceding the $\delta^{18}O$ minimum at 24 Ma, similar to the SST trend at Site U1356. For the mid-Miocene, BWT records of both Site 747 (Kerguelen Plateau) and Site 1171 (South Tasman Rise) show slowly decreasing trends consistent with decreasing TEX_{86}-based SSTs of Site U1356. The similarities of the three Mg/Ca records to our TEX_{86}-based SST record support the transfer of a regional SST signal towards the deep ocean through deep-water formation. However, the temperature

595 differences between temperature optima (e.g., the late Oligocene and MCO) and minima (e.g., the mid-Oligocene and MCT) are much larger for the TEX_{86}-based SSTs than for the Mg/Ca-based BWTs. This difference in the degree of change could be explained by the fact that the formation of deep waters during winter is constrained at the lower end by the freezing point of water, which would limit the degree of change during relatively cold intervals. The degree of change could also be reduced by a shift in the location of deep-water formation to higher latitudes during

600 warmer intervals.

Alternatively, long-term SST trends as well as Southern Ocean BWT trends (Sites 747 and 1171) are governed by large-scale tectonic processes, such as the opening and closure of the Drake Passage, as was suggested by Lagabrielle et al. (2009). Opening of the Drake Passage could result in increased isolation of the Antarctic continent through the establishment of a (proto-)ACC. In turn, this would result in effective blocking of northerly sourced

605 warmer waters as well as ice sheet expansion thereby resulting in a simultaneous benthic $\delta^{18}O$ increase and SST decrease.

As an alternative hypothesis, reconstructed SSTs at Wilkes Land may depend on the volume of the ice sheet in the hinterland. In that scenario most of the long-term trends in the $\delta^{18}O$ record is due to ice volume growth and decline. A more expanded ice sheet will lower SSTs and enhance the formation of sea ice around Antarctica (Goldner et al.,

610 2014). Expansion of this cool (proto-)AASW and the ocean frontal systems to lower latitudes during glacials may have cooled SSTs at Site U1356, while ice-volume decrease and the retreat of the ocean frontal systems during interglacials may have resulted in warmer SSTs at Site U1356. However, the warmth of even the glacial SSTs in our SST record, as well as the overall absence of sea-ice indicators during most of the Oligocene in these glacial intervals, strongly argues against this alternative. Only during the MCT, where dinoflagellate cysts and IRD suggest

615 an increased influence of icebergs or sea ice (Sangiorgi et al., 2018), the ice sheet may have been large enough during the glacial periods to allow the influence of cool (proto-)AASW at Site U1356.

4.3 Sea surface temperature variability at glacial–interglacial time scales

For the Oligocene, the offset between the glacial and interglacial LOESS curves is constant over time (Fig. 4). Irrespective of the chosen calibration (i.e. TEX_{86} or BAYSPAR), SSTs are on average 1.5-3.1°C higher during

620   interglacial intervals than during adjacent glacial times. This glacial-interglacial SST difference is smaller than the observed amplitude of the variability in our temperature record ($2\sigma = 3.6°C$ before 27 Ma), because it takes relatively warm glacials and cool interglacial SST values into account. Also considering that part of the 2σ variability is due to the relatively large calibration error of the BAYSPAR calibration (±4.0°C), the difference of 1.5-3.1°C may be a better representation of average glacial-interglacial SST variation than the 2σ.

625   The average consistent offset between glacial and interglacial values seems to disappear for each of the Miocene data clusters at ~17, ~13.5, and ~10.5 Ma. Several causes could explain this. It could be the result of a less variable climate during the Miocene, which causes both subsets to overlap more. Indeed, for the MCO this may be the case, because the MCO is a time interval of exceptional warmth, with retreated ice sheets and vegetated coastlines of Wilkes Land (Sangiorgi et al., 2018). In such a climate, the glacial intervals may not have been fundamentally

630   colder than the interglacials. We cannot, however, explain the apparent absence of glacial interglacial-temperature variability around 14 and 10.5 Ma, where dinoflagellate cysts suggest profound variability in sea-ice extent, upwelling and temperature (Sangiorgi et al., 2018). It could be that the samples taken by Sangiorgi et al. (2018) do not capture the true glacial and interglacial extremes, but this cannot be verified at this stage. Because a detailed lithological log was not available to Sangiorgi et al. (2018), there is also an uneven distribution between glacial and

635   interglacial samples.

        If the recorded glacial-interglacial SST variability in the Oligocene is representative for the SST variability at the region of deep-water formation, it should be considered when interpreting benthic foraminiferal $\delta^{18}O$ records in terms of ice-volume variability. As such, a larger part of the variability of $\delta^{18}O$ than so far assumed (Hauptvogel et al., 2017; Liebrand et al., 2017;) should be ascribed to deep-sea temperature rather than ice-volume changes. If the

640   region of deep-water formation experienced the same SST variability, 40-70% of the 1‰ deep-sea $\delta^{18}O$ variability over Oligocene glacial-interglacial cycles can be related to deep-sea temperature. However, it is plausible that not the entire range of SST variability is relayed to the deep-sea, and that in the more southerly positioned Ross Sea, the most likely region of Oligocene deep-water formation, temperatures were not as variable as in the Wilkes Land sector. Indeed, Mg/Ca-based reconstructed bottom-water temperatures from Site 1218 show much less glacial-

645   interglacial variation (1.1°C, Fig. 5) (Lear et al., 2004) than our record. Still, our record provides evidence that polar SST experienced considerable variability, both on the short-term glacial-interglacial cycles as well as on the long-term.

        A considerable influence of deep-sea temperature on benthic $\delta^{18}O$ could explain the level of symmetry in glacial-interglacial cycles in the Oligocene (Liebrand et al., 2017), as the temperature would vary in a sinusoidal fashion,

650   whereas ice sheets would respond non-linearly to climate forcing. The sedimentary record of Site U1356 lacks the potential of obtaining a resolution comparable to those of deep-sea $\delta^{18}O$ records, in order to verify these claims. However, ice-volume reconstructions from $\delta^{18}O$ records on both long-term and short-term time scales should consider that an important component of the signal could potentially be ascribed to temperature variability.

5 Conclusions

655 We reconstruct (summer-biased) SSTs of around 17°C on average for the Wilkes Land Margin during the Oligocene, albeit with a high degree of variability (up to a 6.8°C double standard deviation during the late Oligocene). The reconstructed temperatures are a few degrees higher than previously published high-latitude early Oligocene Southern Ocean estimates. Because alternations in the lithology reflect glacial-interglacial cycles, an estimated temperature difference of 1.5 to 3.1°C between glacials and interglacials could be interpreted for the

660 Oligocene. The long-term trends of both glacial and interglacial records show a temperature increase towards 30.5 Ma, followed by a minimum around 27 Ma, an optimum around 25 Ma and finally a decrease towards the end of the Oligocene, generally following the long-term trends in the global benthic δ^{18}O record as well as parts of the available Mg/Ca-based BWT records for the Oligocene. Recalibrated SSTs based on previously published TEX$_{86}$ data for the mid-Miocene decrease from around 17°C to 11°C between ~17 and ~10.5 Ma. A distinct glacial-

665 interglacial SST difference was not observed for the mid-Miocene. Nevertheless, the recorded temperature decline also follows the trend observed in benthic δ^{18}O and Mg/Ca-based BWT records. Our results suggest that considerable SST variability prevailed during the Oligocene and Miocene. This may have implications for the dynamics of marine-based ice sheets, if present, and the extent of the Antarctic ice sheet in general. Assuming that the reconstructed SST trends and glacial-interglacial variability have been relayed to the deep water at nearby

670 bottom-water formation sites, our results indicate that the long-term δ^{18}O trend may be controlled for a considerable part by bottom-water temperature. This implies that the Antarctic Ice Sheet was less dynamic during the Oligocene and Miocene, which could be due to the presence of relatively more land-based versus marine-based ice.

6 Acknowledgements

JDH, FS, HB and PKB acknowledge NWO Netherlands Polar Program project number 866.10.110. SS was

675 supported by the Netherlands Earth System Science Centre (NESSC), funded by the Dutch Ministry of Education, Culture and Science (OCW). PKB and FP received funding through NWO-ALW VENI grant no 863.13.002 and 863.13.016, respectively. CE and AS thank the Spanish Ministerio de Econimía y Competitividad for Grant CTM2014-60451-C2-1-P. We thank Alexander Ebbing and Anja Bruls for GDGT sample preparation during their MSc research. We thank Stephen Gallagher and two anonymous reviewers for their thorough review and

680 constructive comments, which helped improving this manuscript.

7 Author contributions

FS, PKB, HB and SS designed the research. JDH, PKB and AJPH carried out Oligocene GDGT analyses. CE and AS incorporated the lithological data. PKB, FP and SS assisted in GDGT analytical procedures and interpretation. JDH wrote the paper with input from all authors.

8 References

Austermann, J., Pollard, D., Mitrovica, J.X., Moucha, R., Forte, A.M., DeConto, R.M., Rowley, D.B., Raymo, M.E., 2015. The impact of dynamic topography change on Antarctic ice sheet stability during the mid-Pliocene warm period. Geology 43, 927–930. https://doi.org/10.1130/G36988.1

Baines, P.G., 2009. A model for the structure of the Antarctic Slope Front. Deep. Res. Part II 56, 859–873. https://doi.org/10.1016/j.dsr2.2008.10.030

Barker, P.F., Filippelli, G.M., Florindo, F., Martin, E.E., Scher, H.D., 2007. Onset and role of the Antarctic Circumpolar Current. Deep Sea Res. Part II Top. Stud. Oceanogr. 54, 2388–2398. https://doi.org/10.1016/j.dsr2.2007.07.028

Basse, A., Zhu, C., Versteegh, G.J.M., Fischer, G., Hinrichs, K.-U., 2014. Distribution of intact and core tetraether lipids in water column profiles of suspended particulate matter off Cape Blanc , NW Africa. Org. Geochem. 72, 1–13. https://doi.org/10.1016/j.orggeochem.2014.04.007

Beddow, H.M., Liebrand, D., Sluijs, A., Wade, B.S., Lourens, L.J., 2016. Global change across the Oligocene-Miocene transition: High-resolution stable isotope records from IODP Site U1334 (equatorial Pacific Ocean). Paleoceanography 31, 81–97. https://doi.org/10.1002/2015PA002820.Received

Bijl, P.K., Bendle, J.A.P., Bohaty, S.M., Pross, J., Schouten, S., Tauxe, L., Stickley, C.E., McKay, R.M., Röhl, U., Olney, M., Sluijs, A., Escutia, C., Brinkhuis, H., 2013. Eocene cooling linked to early flow across the Tasmanian Gateway. Proc. Natl. Acad. Sci. U. S. A. 110, 9645–9650. https://doi.org/10.1073/pnas.1220872110

Bijl, P.K., Pross, J., Warnaar, J., Stickley, C.E., Huber, M., Guerstein, R., Houben, A.J.P., Sluijs, A., Visscher, H., Brinkhuis, H., 2011. Environmental forcings of Paleogene Southern Ocean dinoflagellate biogeography. Paleoceanography 26, PA1202. https://doi.org/10.1029/2009PA001905

Bijl, P.K., Houben, A.J.P., Bruls, A., Hartman, J.D., Pross, J., Salabarnada, A., Escutia, C., Sangiorgi, F., submitted this volume. Oligocene–Miocene paleoceanography off the Wilkes Land Margin (East Antarctica) based on organic-walled dinoflagellate cysts.

Bijl, P.K., Houben, A.J.P., Bruls, A., Pross, J., Sangiorgi, F., 2018. Stratigraphic calibration of Oligocene-Miocene organic-walled dinoflagellate cysts from offshore Wilkes Land, East Antarctica and a zonation proposal. J. Micropalaeontology 37, 105–138.

Billups, K., Schrag, D.P., 2002. Paleotemperatures and ice volum of the past 27 Myr revisited with paired Mg/Ca and $^{18}O/^{16}O$ measurements on benthic foraminifera. Paleoceanography 17(1), 1003.

Billups, K., Pälike, H., Channell, J.E.T., Zachos, J.C., Shackleton, N.J., 2004. Astronomic calibration of the late Oligocene through early Miocene geomagnetic polarity time scale. Earth Planet. Sci. Lett. 224, 33–44.

Blaga, C.I., Reichart, G.-J., Heiri, O., Sinninghe Damsté, J.S., 2009. Tetraether membrane lipid distributions in water-column particulate matter and sediments: a study of 47 European lakes along a north–south transect. J. Paleolimnol. 41, 523–540. https://doi.org/10.1007/s10933-008-9242-2

Borrelli, C., Katz, M.E., 2015. Dynamic deepwater circulation in the northwestern Pacific during the Eocene: Evidence from ODP Site 884 benthic foraminiferal stable isotopes (δ18O and δ13C). Geosphere, 11, 1204–

1225. doi:10.1130/GES01152.1.

Carter, L., Carter, R.M., McCave, I.N., 2004. Evolution of the sedimentary system beneath the deep Pacific inflow off eastern New Zealand. Mar. Geol. 205, 9–27. https://doi.org/10.1016/S0025-3227(04)00016-7

725   Church, M.J., DeLong, E.F., Ducklow, H.W., Karner, M.B., Preston, C.M., Karl, D.M., 2003. Abundance and distribution of planktonic Archaea and Bacteria in the waters west of the Antarctic Peninsula. Limnol. Oceanogr. 48, 1893–1902. https://doi.org/10.4319/lo.2003.48.5.1893

Church, M.J., Wai, B., Karl, D.M., DeLong, E.F., 2010. Abundances of crenarchaeal amoA genes and transcripts in the Pacific Ocean. Environ. Microbiol. 12, 679–688. https://doi.org/10.1111/j.1462-2920.2009.02108.x

730   Cleveland, W. S., Grosse, E., Shyu, W. M., 1992. Local regression models. In Chambers, J. M. and Hastie, T. J. (eds.) , Statistical Models in S, chapter 8, 309–376. Chapman & Hall, New York.

Cramer, B.S., Toggweiler, J.R., Wright, J.D., Katz, M.E., Miller, K.G., 2009. Ocean overturning since the late cretaceous: Inferences from a new benthic foraminiferal isotope compilation. Paleoceanography 24, 1–14. https://doi.org/10.1029/2008PA001683

735   Crampton, J.S., Cody, R.D., Levy, R., Harwood, D., Mckay, R., Naish, T.R., 2016. Southern Ocean phytoplankton turnover in response to stepwise Antarctic cooling over the past 15 million years 113. https://doi.org/10.1073/pnas.1600318113

Dalziel, I.W.D., 2014. Drake Passage and the Scotia arc: A tortuous space-time gateway for the Antarctic Circumpolar Current. Geology 42, 367–368. https://doi.org/10.1130/focus042014.1

740   Deconto, R.M., Pollard, D., 2016. Contribution of Antarctica to past and future sea-level rise. Nature 531, 591–597. https://doi.org/10.1038/nature17145

DeConto, R.M., Pollard, D., Wilson, P.A., Pälike, H., Lear, C.H., Pagani, M., 2008. Thresholds for Cenozoic bipolar glaciation. Nature 455, 652–656. https://doi.org/10.1038/nature07337

Douglas, P.M.J., Affek, H.P., Ivany, L.C., Houben, A.J.P., Sijp, W.P., Sluijs, A., Schouten, S., Pagani, M., 2014.
745   Pronounced zonal heterogeneity in Eocene southern high-latitude sea surface temperatures. Proc. Natl. Acad. Sci. U. S. A. 111, 1–6. https://doi.org/10.1073/pnas.1321441111

Elderfield, H., Yu, J., Anand, P., Kiefer, T., Nyland, B., 2006. Calibrations for benthic foraminiferal Mg/Ca paleothermometry and the carbonate ion hypothesis. Earth Planet. Sci. Lett. 250, 633–649. https://doi.org/10.1016/j.epsl.2006.07.041

750   Elling, F.J., Könneke, M., Lipp, J.S., Becker, K.W., Gagen, E.J., Hinrichs, K.-U., 2014. Effects of growth phase on the membrane lipid composition of the thaumarchaeon *Nitrosopumilus maritimus* and their implications for archaeal lipid distributions in the marine environment. Geochim. Cosmochim. Acta 141, 579–597.

Elling, F.J., Könneke, M., Mußmann, M., Greve, A., Hinrichs, K.-U., 2015. Influence of temperature, pH, and salinity on membrane lipid composition and TEX_{86} of marine planktonic thaumarchaeotal isolates.
755   Geochim. Cosmochim. Acta 171, 238–255.

Escutia, C., Brinkhuis, H., Klaus, A., the Expedition 318 Scientists, 2011. Expedition 318 summary. Proc. Integr. Ocean Drill. Progr. 318, 1–59. https://doi.org/10.2204/iodp.proc.318.101.2011

Esper, O., Zonneveld, K.A.F., 2007. The potential of organic-walled dinoflagellate cysts for the reconstruction of

past sea-surface conditions in the Southern Ocean. Mar. Micropaleontol. 65, 185–212.

760   Flower, B.P., Kennett, J.P., 1993. Middle Miocene Ocean-Climate Transition: High-resolution oxygen and carbon isotopic records from Deep Sea Drilling Project Site 588A, Southwest Pacific. Paleoceanography 8(6), 811–843.

Fogwill, C.J., Turney, C.S.M., Meissner, K.J., Golledge, N.R., Spence, P., Roberts, J.L., England, M.H., Jones, R.T., Carter, L., 2014. Testing the sensitivity of the East Antarctic Ice Sheet to Southern Ocean dynamics: past

765   changes and future implications. J. Quat. Sci. 29, 91–98. https://doi.org/10.1002/jqs.2683

Ford, H.L., Sodian, S.M., Rosenthal, Y., Raymo, M.E., 2016. Gradual and abrupt changes during the Mid-Pleistocene Transition. Quat. Sci. Rev. 148, 222–233.

Foster, G.L., Rohling, E.J., 2013. Relationship between sea level and climate forcing by CO2 on geological timescales. Proc. Natl. Acad. Sci. 110, 1209–1214. https://doi.org/10.1073/pnas.1216073110

770   Fretwell, P., Pritchard, H.D., Vaughan, D.G., Bamber, J.L., Barrand, N.E., Bell, R., Bianchi, C., Bingham, R.G., Blankenship, D.D., Casassa, G., Catania, G., Callens, D., Conway, H., Cook, A.J., Corr, H.F.J., Damaske, D., Damm, V., Ferraccioli, F., Forsberg, R., Fujita, S., Gim, Y., Gogineni, P., Griggs, J.A., Hindmarsh, R.C.A., Holmlund, P., Holt, J.W., Jacobel, R.W., Jenkins, A., Jokat, W., Jordan, T., King, E.C., Kohler, J., Krabill, W., Riger-Kusk, M., Langley, K.A., Leitchenkov, G., Leuschen, C., Luyendyk, B.P., Matsuoka,

775   K., Mouginot, J., Nitsche, F.O., Nogi, Y., Nost, O.A., Popov, S. V., Rignot, E., Rippin, D.M., Rivera, A., Roberts, J., Ross, N., Siegert, M.J., Smith, A.M., Steinhage, D., Studinger, M., Sun, B., Tinto, B.K., Welch, B.C., Wilson, D., Young, D.A., Xiangbin, C., Zirizzotti, A., 2013. Bedmap2: Improved ice bed, surface and thickness datasets for Antarctica. Cryosphere 7, 375–393. https://doi.org/10.5194/tc-7-375-2013

Gallagher, S.J., Villa, G., Drysdale, R.N., Wade, B.S., Scher, H., Li, Q., Wallace, M.W., Holdgate, G.R., 2013. A

780   near-field sea level record of East Antarctic Ice Sheet instability from 32 to 27 Myr. Paleoceanography 28, 1–13.

Gasson, E., Deconto, R.M., Pollard, D., Levy, R.H., 2016. Dynamic Antarctic ice sheet during the early to mid-Miocene. https://doi.org/10.1073/pnas.1516130113

Goldner, A., Herold, N., Huber, M., 2014. Antarctic glaciation caused ocean circulation changes at the Eocene–

785   Oligocene transition. Nature 511, 574–577. https://doi.org/10.1038/nature13597

Golledge, N.R., Levy, R.H., Mckay, R.M., Naish, T.R., 2017. East Antarctic ice sheet most vulnerable to Weddell Sea warming. Geophys. Res. Lett. 44, 2343–2351. https://doi.org/10.1002/2016GL072422

Gradstein, F.M., Ogg, J.G., Smith, A.G. (Eds.), 2004. A Geologic Time Scale 2004. Cambridge University Press, Cambridge, p. 589.

790   Gradstein, F.M., Ogg, J.G., Schmitz, M.D., Ogg, G. (Eds.), 2012. The Geologic Time Scale 2012. Elsevier, Boston, USA, p. 1127, DOI: 10.1016/B978-0-444-59425-9.00004-4.

Greenbaum, J.S., Blankenship, D.D., Young, D. a, Richter, T.G., Roberts, J.L., Aitken, a R. a, Legresy, B., Schroeder, D.M., Warner, R.C., van Ommen, T.D., Siegert, M.J., 2015. Ocean access to a cavity beneath Totten Glacier in East Antarctica. Nat. Geosci. 8, 1–5. https://doi.org/10.1038/NGEO2388

795   Hauptvogel, D.W., Pekar, S.F., Pincay, V., 2017. Evidence for a heavily glaciated Antarctica during the late

Oligocene "warming" (27.8-24.5 Ma): Stable isotope records from ODP Site 690. Paleoceanography 32, 384–396. https://doi.org/10.1002/2016PA002972

Hill, D.J., Haywood, A.M., Valdes, P.J., Francis, J.E., Lunt, D.J., Wade, B.S., Bowman, V.C., 2013. Paleogeographic controls on the onset of the Antarctic circumpolar current. Geophys. Res. Lett. 40, 5199–5204. https://doi.org/10.1002/grl.50941

Hinsbergen, D.J.J. Van, Groot, L.V. De, Schaik, S.J. Van, Spakman, W., Bijl, P.K., Sluijs, A., Langereis, C.G., Brinkhuis, H., 2015. A Paleolatitude Calculator for Paleoclimate Studies. PLoS One 10, 1–21. https://doi.org/10.5281/zenodo.16166.

Ho, S.L., Laepple, T., 2016. Flat meridional temperature gradient in the early Eocene in the subsurface rather than surface ocean. Nat. Geosci. 9, 606–610. https://doi.org/10.1038/ngeo2763

Ho, S.L., Mollenhauer, G., Fietz, S., Martínez-Garcia, A., Lamy, F., Rueda, G., Schipper, K., Méheust, M., Rosell-Melé, A., Stein, R., Tiedemann, R., 2014. Appraisal of TEX86 and TEX86L thermometries in subpolar and polar regions. Geochim. Cosmochim. Acta 131, 213–226. https://doi.org/10.1016/j.gca.2014.01.001

Holbourn, A., Kuhnt, W., Schulz, M., Flores, J.-A., Andersen, N., 2007. Orbitally-paced climate evolution during the middle Miocene "Monterey" carbon-isotope excursion. Earth Planet. Sci. Let. 261, 534–550.

Holbourn, A., Kuhnt, W., Clemens, S., Prell, W., Andersen, N., 2013. Middle to late Miocene stepwise climate cooling: Evidence from a high-resolution deep water isotope curve spanning 8 million years. Paleoceanography 28, 688–699.

Holbourn, A., Kuhnt, W., Kochhann, K.G.D., Andersen, N., Meier, K.J.S., 2015. Global perturbation of the carbon cycle at the onset of the Miocene Climatic Optimum. Geology 43(2), 123–126.

Hopmans, E.C., Schouten, S., Sinninghe Damsté, J.S., 2016. Organic Geochemistry The effect of improved chromatography on GDGT-based palaeoproxies. Org. Geochem. 93, 1–6. https://doi.org/10.1016/j.orggeochem.2015.12.006

Hopmans, E.C., Weijers, J.W.H., Schefuß, E., Herfort, L., Sinninghe Damsté, J.S., Schouten, S., 2004. A novel proxy for terrestrial organic matter in sediments based on branched and isoprenoid tetraether lipids. Earth Planet. Sci. Lett. 224, 107–116. https://doi.org/10.1016/j.epsl.2004.05.012

Houben, A.J.P., Bijl, P.K., Guerstein, G.R., Sluijs, A.,Brinkhuis, H., 2011. Malvinia escutiana, a new biostratigraphically important Oligocene dinoflagellate cyst from the Southern Ocean. Rev. Palaeobot. Palynol. 165, 175-182. http://dx.doi.org/10.1016/j.revpalbo.2011.03.002

Houben, A.J.P., Bijl, P.K., Pross, J., Bohaty, S.M., Passchier, S., Stickley, C.E., Röhl, U., Sugisaki, S., Tauxe, L., van de Flierdt, T., Olney, M., Sangiorgi, F., Sluijs, A., Escutia, C., Brinkhuis, H., Dotti, C.E., Klaus, A., Fehr, A., Williams, T., Bendle, J. a P., Carr, S. a, Dunbar, R.B., Flores, J.-A., Gonzàlez, J.J., Hayden, T.G., Iwai, M., Jimenez-Espejo, F.J., Katsuki, K., Kong, G.S., McKay, R.M., Nakai, M., Pekar, S.F., Riesselman, C., Sakai, T., Salzmann, U., Shrivastava, P.K., Tuo, S., Welsh, K., Yamane, M., 2013. Reorganization of Southern Ocean plankton ecosystem at the onset of Antarctic glaciation. Science 340, 341–344.

Huck, C.E., van de Flierdt, T., Bohaty, S.M., Hammond, S.J., 2017. Antarctic climate, Southern Ocean circulation patterns and deep water formation during the Eocene. Paleoceanography 32, 674–691.

Huguet, C., Hopmans, E.C., Febo-Ayala, W., Thompson, D.H., Sinninghe Damsté, J.S., Schouten, S., 2006. An improved method to determine the absolute abundance of glycerol dibiphytanyl glycerol tetraether lipids. Org. Geochem. 37, 1036–1041.

Huguet, C., Schimmelmann, A., Thunell, R., Lourens, L.J., Sinninghe Damsté, J.S., Schouten, S., 2007. A study of the TEX$_{86}$ paleothermometer in the water column and sediments of the Santa Barbara Basin, California. Paleoceanography 22, PA3203.

Huguet, C., Kim, J.-H., de Lange, G. J., Sinninghe Damsté, J.S., Schouten, S., 2009. Effects of long term oxic degradation on the U$^{k'}_{37}$, TEX$_{86}$ and BIT organic proxies. Org. Geochem. 40, 1188–1194.

Hurley, S.J., Elling, F.J., Könneke, M., Buchwald, C., Wankel, S.D., Santoro, A.E., Lipp, J.S., Hinrichs, K.-U., Pearson, A., 2016. Influence of ammonia oxidation rate on thaumarchaeotal lipid composition and the TEX$_{86}$ temperature proxy. PNAS 113(28), 7762–7767.

Hutcheon, J.A., Chiolero, A., Hanley, J.A., 2010. Random measurements error and regression dilution bias. BMJ 340, c2289.

IPCC, 2014. Climate Change 2014: Synthesis Report. Contribution of Working Groups I, II and III to the Fifth Assessment Report of the Intergovernmental Panel on Climate Change. IPCC, Geneva, Switzerland.Jacobs, S.S., 1991. On the nature and significance of the Antarctic Slope Front. Mar. Chem. 35, 9–24. https://doi.org/10.1016/S0304-4203(09)90005-6

John, C.M., Karner, G.D., Browning, E., Leckie, R.M., Mateo, Z., Carson, B., Lowery, C., 2011. Timing and magnitude of Miocene eustacy derived from the mixed siliciclastic-carbonate stratigraphic record of the northeastern Australian margin. Earth Planet. Sci. Lett. 304, 455–467.

Joughin, I., Smith, B.E., Medley, B., 2014. Marine Ice Sheet Collapse Potentially Under Way for the Thwaites Glacier Basin, West Antarctica. Science (80-.). 344, 735–738. https://doi.org/10.1126/science.1249055

Kalanetra, K.M., Bano, N., Hollibaugh, J.T., 2009. Ammonia-oxidizing Archaea in the Arctic Ocean and Antarctic coastal waters. Environ. Microbiol. 11, 2434–2445. https://doi.org/10.1111/j.1462-2920.2009.01974.x

Karner, M.B., DeLong, E.F., Karl, D.M., 2001. Archaeal dominance in the mesopelagic zone of the Pacific Ocean. Nature 409, 507–510. https://doi.org/10.1038/35054051

Katz, M.E., Cramer, B.S., Toggweiler, J.R., Esmay, G., Liu, C., Miller, K.G., Rosenthal, Y., Wade, B.S., Wright, J.D., 2011. Impact of Antarctic Circumpolar Current development on late Paleogene ocean structure. Science (80-.). 332, 1076–1079. https://doi.org/10.1126/science.1202122

Kelson, J.R., Huntington, K.W., Schauer, A.J., Saenger, C., Lechler, A.R., 2017. Toward a universal carbonate clumped isotope calibration : Diverse synthesis and preparatory methods suggest a single temperature relationship. Geochim. Cosmochim. Acta 197, 104–131. https://doi.org/10.1016/j.gca.2016.10.010

Kim, J.-H., Crosta, X., Willmott, V., Renssen, H., Bonnin, J., Helmke, P., Schouten, S., Sinninghe Damsté, J.S., 2012a. Holocene subsurface temperature variability in the eastern Antarctic continental margin. Geophys. Res. Lett. 39. https://doi.org/10.1029/2012GL051157

Kim, J.-H., Huguet, C., Zonneveld, K.A.F., Versteegh, G.J.M., Roeder, W., Sinninghe Damsté, J.S., Schouten, S., 2009. An experimental field study to test the stability of lipids used for the TEX$_{86}$ and U$^{K'}_{37}$

870   palaeothermometers. Geochim. Cosmochim. Acta 73, 2888–2898.

Kim, J.-H., Romero, O.E., Lohmann, G., Donner, B., Laepple, T., Haam, E., Damsté, J.S.S., 2012b. Pronounced subsurface cooling of North Atlantic waters off Northwest Africa during Dansgaard – Oeschger interstadials. Earth Planet. Sci. Lett. 339–340, 95–102. https://doi.org/10.1016/j.epsl.2012.05.018

Kim, J.-H., Schouten, S., Hopmans, E.C., Donner, B., Sinninghe Damsté, J.S., 2008. Global sediment core-top
875   calibration of the TEX86 paleothermometer in the ocean. Geochim. Cosmochim. Acta 72, 1154–1173. https://doi.org/10.1016/j.gca.2007.12.010

Kim, J.-H., Schouten, S., Rodrigo-Gámiz, M., Rampen, S., Marino, G., Huguet, C., Helmke, P., Buscail, R., Hopmans, E.C., Pross, J., Sangiorgi, F., Middelburg, J.B.M., Sinninghe Damsté, J.S., 2015. Influence of deep-water derived isoprenoid tetraether lipids on the TEX_{86}^{H} paleothermometer in the Mediterranean Sea.
880   Geochim. Cosmochim. Acta 150, 125–141.

Kim, J.-H., van der Meer, J., Schouten, S., Helmke, P., Willmott, V., Sangiorgi, F., Koç, N., Hopmans, E.C., Damsté, J.S.S., 2010. New indices and calibrations derived from the distribution of crenarchaeal isoprenoid tetraether lipids: Implications for past sea surface temperature reconstructions. Geochim. Cosmochim. Acta 74, 4639–4654. https://doi.org/10.1016/j.gca.2010.05.027 Kim, J.-H., Villanueva, L., Zell, C., Sinninghe
885   Damsté, J.S., 2016. Biological source and provenance of deep-water derived isoprenoid tetraether lipids along the Portuguese continental margin. Geochim. Cosmochim. Acta 172, 177–204. https://doi.org/10.1016/j.gca.2015.09.010

Koga, Y., Morii, H., Akagawa-Matsushita, M., Ohga, M., 1998. Correlation of Polar Lipid Composition with 16S rRNA Phylogeny in Methanogens. Further Analysis of Lipid Component Parts. Bioscience, Biotechnology
890   and Biochemistry 62(2), 230-236.

Kuhnert, H., Bickert, T., Paulsen, H., 2009. Southern Ocean frontal system changes precede Antarctic ice sheet growth during the middle Miocene. Earth and Planetary Science Letters 284, 630–638.

Lagabrielle, Y., Malavieille, J., Suárez, M., 2009. The tectonic history of Drake Passage and its possible impacts on global climate. Earth Planet. Sci. Lett. 279, 197–211. https://doi.org/10.1016/j.epsl.2008.12.037
895 Lawver, L.A., Gahagan, L.M., 2003. Evolution of cenozoic seaways in the circum-antarctic region. Palaeogeogr. Palaeoclimatol. Palaeoecol. 198, 11–37. https://doi.org/10.1016/S0031-0182(03)00392-4

Lear, C.H., Mawbey, E.M., Rosenthal, Y., 2010. Cenozoic benthic foraminiferal Mg/Ca and Li/Ca records: Toward unlocking temperatures and saturation states. Paleoceanography 25, 1–11. https://doi.org/10.1029/2009PA001880
900 Lear, C.H., Rosenthal, Y., Coxall, H.K., Wilson, P.A., 2004. Late Eocene to early Miocene ice sheet dynamics and the global carbon cycle. Paleoceanography 19, PA4015. https://doi.org/10.1029/2004PA001039

Lear, C.H., Coxall, H.K., Foster, G.L., Lunt, D.J., Mawbey, E.M., Rosenthal, Y., Sosdian, S.M., Thomas, E., Wilson, P.A., 2015. Neogene ice volume and ocean temperature: Insights from infaunal foraminiferal Mg/Ca paleothermometry. Paleoceanography 30, 1437–1454.
905 Levy, R., Harwood, D., Florindo, F., Sangiorgi, F., Tripati, R., von Eynatten, H., Gasson, E., Kuhn, G., Tripati, A., DeConto, R., Fielding, C., Field, B., Golledge, N., McKay, R., Naish, T., Olney, M., Pollard, D., Schouten,

S., Talarico, F., Warny, S., Willmott, V., Acton, G., Panter, K., Paulsen, T., Taviani, M., the SMS Science Team, 2016. Antarctic ice sheet sensitivity to atmospheric CO_2 variations in the early to mid-Miocene. PNAS 113 (13), 3453–3458.

910 Liebrand, D., Bakker, A.T.M. De, Beddow, H.M., Wilson, P.A., Bohaty, S.M., 2017. Evolution of the early Antarctic ice ages. PNAS 114, 3867–3872. https://doi.org/10.1073/pnas.1615440114

Liebrand, D., Beddow, H.M., Lourens, L.J., Pälike, H., Raffi, I., Bohaty, S.M., Hilgen, F.J., Saes, M.J.M., Wilson, P.A., Dijk, A.E. Van, Hodell, D.A., Kroon, D., Huck, C.E., Batenburg, S.J., 2016. Cyclostratigraphy and eccentricity tuning of the early Oligocene oxygen and carbon isotope records from Walvis Ridge Site 1264.

915 Earth Planet. Sci. Lett. 1, 1–14. https://doi.org/10.1016/j.epsl.2016.06.007

Liebrand, D., Lourens, L.J., Hodell, D.A., De Boer, B., Van De Wal, R.S.W., Pälike, H., 2011. Antarctic ice sheet and oceanographic response to eccentricity forcing during the early Miocene. Clim. Past 7, 869–880. https://doi.org/10.5194/cp-7-869-2011

Liu, Z., Pagani, M., Zinniker, D., DeConto, R., Huber, M., Brinkhuis, H., Shah, S.R., Leckie, R.M., Pearson, A.,

920 2009. Global Cooling During the Eocene-Oligocene Climate Transition. Science (80-.). 323, 1187–1190. https://doi.org/10.1126/science.1166368

Livermore, R., Eagles, G., Morris, P., Maldonado, A., 2004. Shackleton Fracture Zone: No barrier to early circumpolar ocean circulation. Geology 32, 797–800. https://doi.org/10.1130/G20537.1

Livermore, R., Hillenbrand, C.-D., Meredith, M., Eagles, G., 2007. Drake Passage and Cenozoic climate: An open

925 and shut case? Geochemistry, Geophys., Geosystems 8(1), Q01005.

Locarnini, R.A., Mishonov, A.V., Antonov, J.I., Boyer, T.P., Garcia, H.E., Baranova, O.K., Zweng, M.M., Johnson, D.R., 2010. World Ocean Atlas 2009, Volume 1 : Temperature, NOAA Atlas NESDIS 68. U.S. Government Printing Office, Washington, D.C.

Lopes dos Santos, R.A., Prange, M., Castañeda, I.S., Schefuß, E., Mulitza, S., Schulz, M., Niedermeyer, E.M.,

930 Sinninghe, J.S., Schouten, S., 2010. Glacial – interglacial variability in Atlantic meridional overturning circulation and thermocline adjustments in the tropical North Atlantic. Earth Planet. Sci. Lett. 300, 407–414. https://doi.org/10.1016/j.epsl.2010.10.030

Lunt, D.J., Valdes, P.J., Jones, T.D., Ridgwell, A., Haywood, A.M., Schmidt, D.N., Marsh, R., Maslin, M., 2010. CO_2-driven ocean circulation changes as an amplifier of Paleocene-Eocene thermal maximum hydrate

935 destabilization. Geology 38(10), 875–878.

Maldonado, A., Bohoyo, F., Galindo-Zaldívar, J., Hernández-Molina, F.J., Lobo, F.J., Lodolo, E., Martos, Y.M., Pérez, L.F., Schreider, A. a., Somoza, L., 2014. A model of oceanic development by ridge jumping: Opening of the Scotia Sea. Glob. Planet. Change 123, 152–173. https://doi.org/10.1016/j.gloplacha.2014.06.010

940 Maldonado, A., Barnolas, A., Bohoyo, F., Escutia, C., Galindo-Zaldívar, J., Hernández-Molina, J., Jabaloy, A., Lobo, F.J., Nelson, C.H., Rodríguez-Fernández, J., Somoza, L., Vázquez, J.-T., 2005. Miocene to Recent contourite drifts development in the northern Weddell Sea (Antarctica). Glob. Planet. Change 45, 99–129.

Maldonado, A., Barnolas, A., Bohoyo, F., Galindo-Zaldívar, J., Hernández-Molina, J., Lobo, F., Rodríguez-Fernández, J., Somoza, L., Vázquez, J.T., 2003. Contourite deposits in the central Scotia Sea: the importance of the Antarctic Circumpolar Current and the Weddell Gyre flows. Palaeogeography, Palaeoclimatology, Palaeoecology 198, 187-221.

Marret, F., De Vernal, A., 1997. Dinoflagellate cyst distribution in surface sediments of the southern Indian Ocean. Mar. Micropaleontol. 29, 367–392.

Majewski, W., Bohaty, S., 2010. Surface-water cooling and salinity decrease during the Middle Miocene climate transition at Southern Ocean ODP Site 747 (Kerguelen Plateau). Mar. Micropaleontol. 74, 1–14.

Markwick, P.J., 2007. The palaeogeographic and palaeoclimatic significance of climate proxies for data-model comparisons, in: Williams, M., Haywood, A., Gregory, F., Schmidt, D.N. (Eds.), Deep-Time Perspectives on Climate Change: Marrying the Signal from Computer Models and Biological Proxies. The Micropalaeontological Society, Special Publications. London, The Geological Society, pp. 251–312.

Mcmillan, M., Shepherd, A., Sundal, A., Briggs, K., Muir, A., Ridout, A., Hogg, A., Wingham, D., 2014. Increased ice losses from Antarctica detected by CryoSat-2. Geophys. Res. Lett. 41, 3899–3906. https://doi.org/10.1002/2014GL060111.Received

Miles, B.W.J., Stokes, C.R., Jamieson, S.S.R., 2016. Pan – ice-sheet glacier terminus change in East Antarctica reveals sensitivity of Wilkes Land to sea-ice changes. Sci. Adv. 2, e1501350.

Miller, K.G., Baluyot, R., Wright, J.D., Kopp, R.E., Browning, J.V., 2017. Closing an early Miocene astronomical gap with Southern Ocean δ^{18}O and δ^{13}C records: Implications for sea level change. Paleoceanography 32, 600–621.

Mollenhauer, G., Basse, A., Kim, J.H., Sinninghe Damsté, J.S., Fischer, G., 2015. A four-year record of UK'37- and TEX86-derived sea surface temperature estimates from sinking particles in the filamentous upwelling region off Cape Blanc, Mauritania. Deep. Res. Part I Oceanogr. Res. Pap. 97, 67–79. https://doi.org/10.1016/j.dsr.2014.11.015

Murray, A.E., Preston, C.M., Massana, R., Taylor, T.L., Blakis, A., Wu, K., Delong, E.F., 1998. Seasonal and spatial variability of bacterial and archaeal assemblages in the coastal waters near Anvers Island, Antarctica. Appl. Environ. Microbiol. 64, 2585–2595.

Naish, T.R., Woolfe, K.J., Barrett, P.J., Wilson, G.S., Atkins, C., Bohaty, S.M., Bücker, C.J., Claps, M., Davey, F.J., Dunbar, G.B., Dunn, A.G., Fielding, C.R., Florindo, F., Hannah, M.J., Harwood, D.M., Henrys, S.A., Krissek, L.A., Lavelle, M., van Der Meer, J., McIntosh, W.C., Niessen, F., Passchier, S., Powell, R.D., Roberts, A.P., Sagnotti, L., Scherer, R.P., Strong, C.P., Talarico, F., Verosub, K.L., Villa, G., Watkins, D.K., Webb, P.N., Wonik, T., 2001. Orbitally induced oscillations in the East Antarctic ice sheet at the Oligocene/Miocene boundary. Nature 413, 719–23. https://doi.org/10.1038/35099534

Orsi, A.H., Whitworth, T., Nowlin, W.D., 1995. On the meridional extent and fronts of the Antarctic Circumpolar Current. Deep Sea Res. Part I Oceanogr. Res. Pap. 42, 641–673. https://doi.org/10.1016/0967-0637(95)00021-W

Pagani, M., Huber, M., Liu, Z., Bohaty, S.M., Henderiks, J., Sijp, W., Krishnan, S., DeConto, R.M., 2011. The Role

980   of Carbon Dioxide During the Onset of Antarctic Glaciation. Science (80-.). 334, 1261–1265. https://doi.org/10.1126/science.1203909

Pälike, H., Frazier, J., Zachos, J.C., 2006a. Extended orbitally forced palaeoclimatic records from the equatorial Atlantic Ceara Rise. Quat. Sci. Rev. 25, 3138–3149.

Pälike, H., Norris, R.D., Herrle, J.O., Wilson, P.A., Coxall, H.K., Lear, C.H., Shackleton, N.J., Tripati, A.K., Wade,
985   B.S., 2006b. The Heartbeat of the Oligocene Climate System. Science (80-.). 314, 1894–1898. https://doi.org/10.1126/science.1133822

Parrenin, F., Masson-Delmotte, V., Köhler, P., Raynaud, D., Paillard, D., Schwander, J., Barbante, C., Landais, A., Wegner, A., Jouzel, J., 2013. Synchronous Change of Atmospheric CO2 and Antarctic Temperature During the Last Deglacial Warming. Science (80-.). 339, 1060–1063.

990   Passchier, S., Krissek, L.A., 2008. Oligocene-Miocene Antarctic continental weathering record and paleoclimatic implications, Cape Roberts drilling Project, Ross Sea, Antarctica. Palaeogeography, Palaeoclimatology, Palaeoecology 260, 30-40.

Pekar, S.F., Christie-Blick, N., 2008. Resolving apparent conflicts between oceanographic and Antarctic climate records and evidence for a decrease in pCO2 during the Oligocene through early Miocene (34–16 Ma).
995   Palaeogeogr. Palaeoclimatol. Palaeoecol. 260, 41–49. https://doi.org/10.1016/j.palaeo.2007.08.019

Pekar, S.F., DeConto, R.M., Harwood, D.M., 2006. Resolving a late Oligocene conundrum: Deep-sea warming and Antarctic glaciation. Palaeogeogr. Palaeoclimatol. Palaeoecol. 231, 29–40. https://doi.org/10.1016/j.palaeo.2005.07.024

Peterse, F., Kim, J., Schouten, S., Klitgaard, D., Koç, N., Sinninghe, J.S., 2009. Constraints on the application of the
1000   MBT / CBT palaeothermometer at high latitude environments (Svalbard , Norway). Org. Geochem. 40, 692–699. https://doi.org/10.1016/j.orggeochem.2009.03.004

Petersen, S. V., Schrag, D.P., 2015. Antarctic ice growth before and after the Eocene-Oligocene Transition: New estimates from clumped isotope paleothermometry. Paleoceanography n/a-n/a. https://doi.org/10.1002/2014PA002769

1005   Plancq, J., Mattioli, E., Pittet, B., Simon, L., Grossi, V., 2014. Productivity and sea-surface temperature changes recorded during the late Eocene-early Oligocene at DSDP Site 511 (South Atlantic). Palaeogeogr. Palaeoclimatol. Palaeoecol. 407, 34–44. https://doi.org/10.1016/j.palaeo.2014.04.016

Pollard, D., Deconto, R.M., Alley, R.B., 2015. Potential Antarctic Ice Sheet retreat driven by hydrofracturing and ice cliff failure. Earth Planet. Sci. Lett. 412, 112–121. https://doi.org/10.1016/j.epsl.2014.12.035

1010   Prebble, J.G., Crouch, E.M., Carter, L., Cortese, G., Bostock, H., Neil, H., 2013. An expanded modern dinoflagellate cyst dataset for the Southwest Pacific and Southern Hemisphere with environmental associations. Mar. Micropaleontol. 101, 33–48. https://doi.org/10.1016/j.marmicro.2013.04.004

Pross, J., Contreras, L., Bijl, P.K., Greenwood, D.R., Bohaty, S.M., Schouten, S., Bendle, J. a, Röhl, U., Tauxe, L., Raine, J.I., Huck, C.E., van de Flierdt, T., Jamieson, S.S.R., Stickley, C.E., van de Schootbrugge, B.,
1015   Escutia, C., Brinkhuis, H., 2012. Persistent near-tropical warmth on the Antarctic continent during the early Eocene epoch. Nature 488, 73–77. https://doi.org/10.1038/nature11300

Qin, W., Carlson, L.T., Armbrust, E.V., Devol, A.H., Moffett, J.W., Stahl, D.A., Ingalls, A.E., 2015. Confounding effects of oxygen and temperature on the TEX_{86} signature of marine Thaumarchaeota. PNAS 112(35), 10979–10984.

1020 Ravelo, A.C., Hillaire-Marcel, C., 2007. The Use of Oxygen and Carbon Isotopes of Foraminifera in Paleoceanography, in: Developments in Marine Geology. Elsevier B.V., pp. 735–764. https://doi.org/10.1016/S1572-5480(07)01023-8

Richey, J.N., Tierney, J.E., 2016. GDGT and alkenone flux in the northern Gulf of Mexico: Implications for the TEX86 and Uk'37 paleothermometers. Paleoceanography 31, 1547–1561.

1025 https://doi.org/10.1002/2016PA003032

Rodrigo-Gámiz, M., Rampen, S.W., de Haas, H., Baas, M., Schouten, S., Sinninghe Damsté, J.S., 2015. Constraints on the applicability of the organic temperature proxies UK'37, TEX86 and LDI in the subpolar region around Iceland. Biogeosciences Discuss. 12, 1113–1153. https://doi.org/10.5194/bgd-12-1113-2015

Salabarnada, A., Escutia, C., Röhl, U., Nelson, C.H., McKay, R., Jiménez-Espejo, F.F., Bijl, P.K., Hartman, J.D.,

1030 Ikehara, M., Strother, S.L., Salzmann, U., Evangelinos, D., López-Quirós, A., Sangiorgi, F., Brinkhuis, H., submitted this volume. Late Oligocene obliquity-paced contourite sedimentation in the Wilkes Land margin of East Antarctica: implications for paleoceanographic and ice sheet configurations.

Sangiorgi, F., Bijl, P.K., Passchier, S., Salzmann, U., Schouten, S., McKay, R., Cody, R.D., Pross, J., van de Flierdt, T., Bohaty, S.M., Levy, R., Williams, T., Escutia, C., Brinkhuis, H., 2018. Southern Ocean warming and

1035 Wilkes Land ice sheet retreat during the mid-Miocene. Nat. Commun. 9, 317.

Scher, H.D., Martin, E.E., 2008. Oligocene deep water export from the North Atlantic and the development of the Antarctic Circumpolar Current examined with neodymium isotopes. Paleoceanography 23, 1–12. https://doi.org/10.1029/2006PA001400

Scher, H.D., Martin, E.E., 2006. Timing and climatic consequences of the opening of Drake Passage. Science (80-.

1040). 312, 428–430. https://doi.org/10.1126/science.1120044

Scher, H.D., Whittaker, J.M., Williams, S.E., Latimer, J.C., Kordesch, W.E.C., Delaney, M.L., 2015. Onset of Antarctic Circumpolar Current 30 million years ago as Tasmanian Gateway aligned with westerlies. Nature 523, 580–583. https://doi.org/10.1038/nature14598

Schnack-Schiel, S.B., 2001. Aspects of the study of the life cycles of Antarctic copepods. Hydrobiologia 453–454,

1045 9–24. https://doi.org/10.1023/A:1013195329066

Schouten, S., Hopmans, E.C., M, E.S., 2002. Distributional variations in marine crenarchaeotal membrane lipids : a new tool for reconstructing ancient sea water temperatures ? Earth Planet. Sci. Lett. 204, 265–274. https://doi.org/10.1016/S0012-821X(02)00979-2

Schouten, S., Hopmans, E.C., Sinninghe Damsté, J.S., 2013. The organic geochemistry of glycerol dialkyl glycerol

1050 tetraether lipids: A review. Org. Geochem. 54, 19–61. https://doi.org/10.1016/j.orggeochem.2012.09.006

Shen, Q., Hansheng, W., Shum, C.K., Jiang, L., Hsu, H.T., Dong, J., 2018. Recent high-resolution Antarctic ice velocity maps reveal increased mass loss in Wilkes Land, East Antarctica. Sci. Rep. 8, 4477.

Shevenell, A.E., Kennett, J.P., Lea, D.W., 2004. Middle Miocene Southern Ocean cooling and Antarctic cryosphere

expansion. Science 305, 1766-1770.

1055 Sinninghe Damsté, J.S., 2016. Spatial heterogeneity of sources of branched tetraethers in shelf systems : The geochemistry of tetraethers in the Berau River delta (Kalimantan , Indonesia). Geochim. Cosmochim. Acta 186, 13–31. https://doi.org/10.1016/j.gca.2016.04.033

Sinninghe Damste, J.S., Ossebaar, J., Abbas, B., Schouten, S., Verschuren, D., 2009. Fluxes and distribution of tetraether lipids in an equatorial African lake : Constraints on the application of the TEX 86

1060 palaeothermometer and BIT index in lacustrine settings. Geochim. Cosmochim. Acta 73, 4232–4249. https://doi.org/10.1016/j.gca.2009.04.022

Sluijs, A., Bijl, P.K., Schouten, S., Röhl, U., Reichart, G.-J., Brinkhuis, H., 2011. Southern ocean warming, sea level and hydrological change during the Paleocene-Eocene thermal maximum. Clim. Past 7, 47–61. https://doi.org/10.5194/cp-7-47-2011

1065 Sorlien, C.C., Luyendyk, B.P., Wilson, D.S., Decesari, R.C., Bartek, L.R., Diebold, J.B., 2007. Oligocene development of the West Antarctic Ice Sheet recorded in eastern Ross Sea strata. Geology 35, 467–470. https://doi.org/10.1130/G23387A.1

Spilling, K., Ylöstalo, P., Simis, S., Seppälä, J., 2015. Interaction Effects of Light , Temperature and Nutrient Limitations (N , P and Si) on Growth , Stoichiometry and Photosynthetic Parameters of the Cold-Water

1070 Diatom Chaetoceros wighamii. PLoS One 10, e0126308. https://doi.org/10.1371/journal.pone.0126308

Stap, L.B., van de Wal, R.S.W., de Boer, B., Bintanja, R., Lourens, L.J., 2017. The influence of ice sheets on temperature during the past 38 million years inferred from a one-dimensional ice sheet-climate model. Clim. Past 13, 1243–1257.

Stickley, C.E., Brinkhuis, H., Schellenberg, S.A., Sluijs, A., Röhl, U., Fuller, M., Grauert, M., Huber, M., Warnaar,

1075 J., Williams, G.L., 2004. Timing and nature of the deepening of the Tasmanian Gateway. Paleoceanography 19, 1–18. https://doi.org/10.1029/2004PA001022

Strother, S.L., Salzmann, U., Sangiorgi, F., Bijl, P.K., Pross, J., Escutia, C., 2017. A new quantitative approach to identify reworking in Eocene to Miocene pollen records from offshore Antarctica using red fluorescence and digital imaging. Biogeosciences 14, 2089–2100. https://doi.org/10.5194/bg-14-2089-2017

1080 Tauxe, L., Stickley, C.E., Sugisaki, S., Bijl, P.K., Bohaty, S.M., Brinkhuis, H., Escutia, C., Flores, J.A., Houben, A.J.P., Iwai, M., Jiménez-Espejo, F., McKay, R., Passchier, S., Pross, J., Riesselman, C.R., Röhl, U., Sangiorgi, F., Welsh, K., Klaus, A., Fehr, A., Bendle, J.A.P., Dunbar, R., Gonzàlez, J., Hayden, T., Katsuki, K., Olney, M.P., Pekar, S.F., Shrivastava, P.K., van de Flierdt, T., Williams, T., Yamane, M., 2012. Chronostratigraphic framework for the IODP Expedition 318 cores from the Wilkes Land Margin:

1085 Constraints for paleoceanographic reconstruction. Paleoceanography 27, PA2214. https://doi.org/10.1029/2012PA002308

Taylor, K.W.R., Huber, M., Hollis, C.J., Hernandez-Sanchez, M.T., Pancost, R.D., 2013. Re-evaluating modern and Palaeogene GDGT distributions: Implications for SST reconstructions. Glob. Planet. Change 108, 158–174. https://doi.org/10.1016/j.gloplacha.2013.06.011

1090 Tierney, J.E., Tingley, M.P., 2015. A TEX 86 surface sediment database and extended Bayesian calibration 1–10.

https://doi.org/10.1038/sdata.2015.29

Tierney, J.E., Tingley, M.P., 2014. A Bayesian, spatially-varying calibration model for the TEX86 proxy. Geochim. Cosmochim. Acta 127, 83–106. https://doi.org/10.1016/j.gca.2013.11.026

Tierney, J.E., Sinninghe Damsté, J.S., Pancost, R.D., Sluijs, A., Zachos, J.C., 2017. Eocene temperature gradients. Nat. Geosci. 10, 538–539.

The IMBRIE Team, 2018. Mass balance of the Antarctic Ice Sheet from 1992 to 2017. Nature 558, 219–222.

Trommer, G., Siccha, M., van der Meer, M.T.J., Schouten, S., Sinninghe Damsté, J.S., Schulz, H., Hemleben, C., Kucera, M., 2009. Organic Geochemistry Distribution of Crenarchaeota tetraether membrane lipids in surface sediments from the Red Sea. Org. Geochem. 40, 724–731. https://doi.org/10.1016/j.orggeochem.2009.03.001

Villanueva, L., Schouten, S., Damsté, J.S.S., Box, P.O., 2015. Depth-related distribution of a key gene of the tetraether lipid biosynthetic pathway in marine Thaumarchaeota 17, 3527–3539. https://doi.org/10.1111/1462-2920.12508

Wang, Xiao-Feng, 2010. fANCOVA: Non-parametric analysis of covariance. https://CRAN.R-project.org/package=fANCOVA

Warnaar, J., 2006. Climatological implications of Australian-Antarctic separation [Ph.D. Thesis], Utrecht University, pp.143.

Weijers, J.W.H., Lim, K.L.H., Aquilina, A., Sinninghe Damsté, J.S., Pancost, R.D., 2011. Biogeochemical controls on glycerol dialkyl glycerol tetraether lipid distributions in sediments characterized by diffusive methane flux. Geochemistry, Geophys. Geosystems 12, Q10010. https://doi.org/10.1029/2011GC003724

Weijers, J.W.H., Schouten, S., Hopmans, E.C., Geenevasen, J.A.J., David, O.R.P., Coleman, J.M., Pancost, R.D., Sinninghe Damsté, J.S., 2006. Membrane lipids of mesophilic anaerobic bacteria thriving in peats have typical archaeal traits. Environ. Microbiol. 8, 648–657. https://doi.org/10.1111/j.1462-2920.2005.00941.x

Westerhold, T., Bickert, T., Röhl, U., 2005. Middle to late Miocene oxygen isotope stratigraphy of ODP site 1085 (SE Atlantic): new constraints on Miocene climate variability and sea-level fluctuations. Palaeogeogr. Palaeoclimatol. Palaeoecol. 217, 205–222.

Wilson, D.S., Jamieson, S.S.R., Barrett, P.J., Leitchenkov, G., Gohl, K., Larter, R.D., 2012. Antarctic topography at the Eocene–Oligocene boundary. Palaeogeogr. Palaeoclimatol. Palaeoecol. 335–336, 24–34. https://doi.org/10.1016/j.palaeo.2011.05.028

Yamamoto, M., Shimamoto, A., Fukuhara, T., Tanaka, Y., Ishizaka, J., 2012. Glycerol dialkyl glycerol tetraethers and TEX86 index in sinking particles in the western North Pacific. Org. Geochem. 53, 52–62. https://doi.org/10.1016/j.orggeochem.2012.04.010

Zachos, J., 2001. Trends, Rhythms, and Aberrations in Global Climate 65 Ma to Present. Science (80-.). 292, 686–693. https://doi.org/10.1126/science.1059412

Zachos, J., Shackleton, N.J., Revenaugh, J.S., Pälike, H., Flower, B.P., 2001. Forcing across the Oligocene-Miocene Boundary. Science 292, 274–278.

Zachos, J.C., Dickens, G.R., Zeebe, R.E., 2008. An early Cenozoic perspective on greenhouse warming and carbon-

cycle dynamics. Nature 451, 279–283. https://doi.org/10.1038/nature06588

Zhang, Y.G., Pagani, M., Liu, Z., Bohaty, S.M., DeConto, R., 2013. A 40-million-year history of atmospheric CO2. Phil. Trans. R. Soc. A 371, 20130096. https://doi.org/10.1098/rsta.2013.0096

Zhang, Y.G., Pagani, M., Wang, Z., 2016. Ring Index: A new strategy to evaluate the integrity of TEX86 paleothermometry. Paleoceanography 31, 220–232. https://doi.org/10.1002/2015PA002848.Received

Zhang, Y.G., Zhang, C.L., Liu, X., Li, L., Hinrichs, K., Noakes, J.E., 2011. Methane Index : A tetraether archaeal lipid biomarker indicator for detecting the instability of marine gas hydrates 307, 525–534. https://doi.org/10.1016/j.epsl.2011.05.031

A. PRESENT

SSST (˚C)

B. 30 Ma

ACCC

PLC
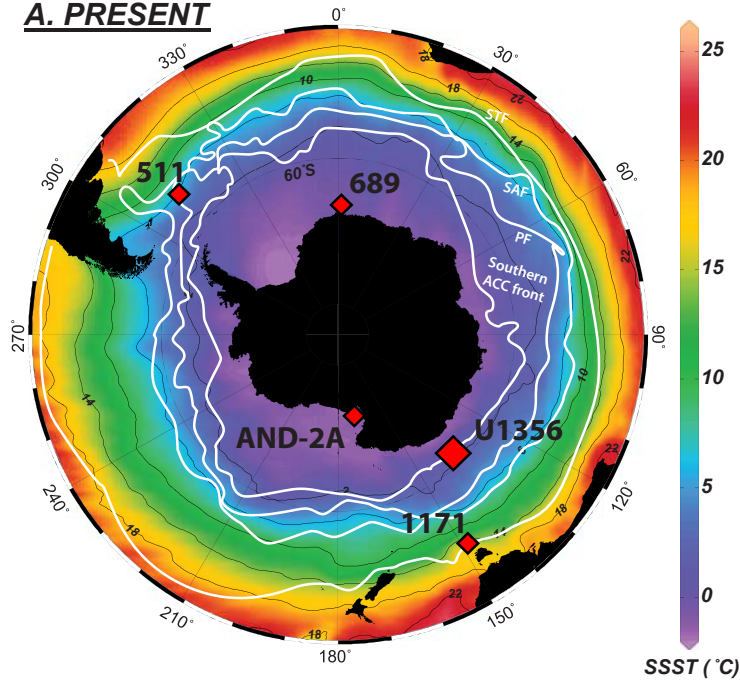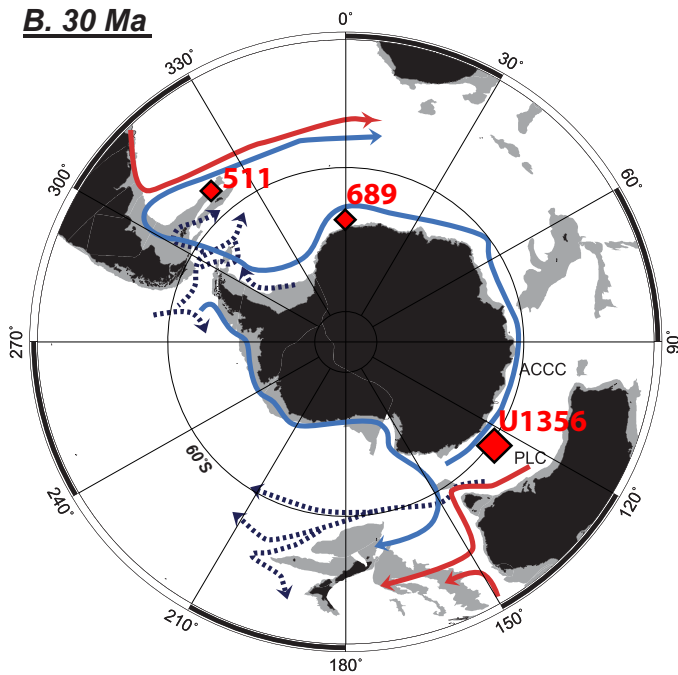
C. 17 Ma
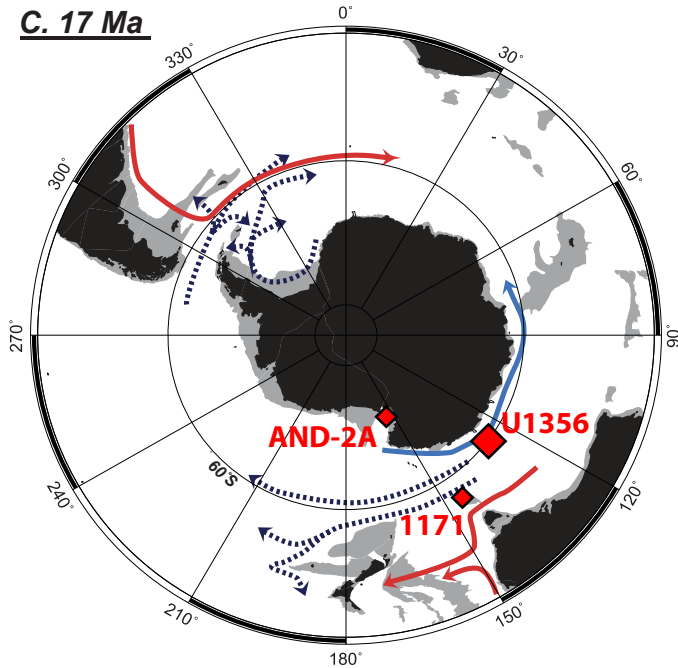
Figure 1: (A) Present-day Southern Ocean summer temperatures and geography obtained from the World Ocean Atlas (Locarnini et al., 2010) using Ocean Data View, and Southern Ocean Fronts obtained from Orsi et al. (1995). PF = Polar Front, SAF = Sub-Antarctic Front, STF = Sub-Tropical Front. Red diamonds indicate DSDP/ODP/IODP Site locations. (B) Modified ODSN-generated map of Antarctica around 30 Ma (continents in black, shelf areas in grey). Paleolatitudes calculated with paleolatitude.org Hinsbergen et al., 2015). Reconstructed cold (light blue) and warm (red) surface currents are based on publications by Stickley et al. (2004), Warnaar (2006), Bijl et al. (2011), Bijl et al., (2013), and Douglas et al. (2014). Reconstructed bottom-water currents (dotted dark blue) are based on publications by Carter et al. (2004), Livermore et al. (2007), Maldonado et al. (2014) and Scher et al. (2015). ACCC = Antarctic Circumpolar Counter Current, PLC = proto-Leeuwin Current. (C) The same as the middle figure, but then for the period around 17 Ma.
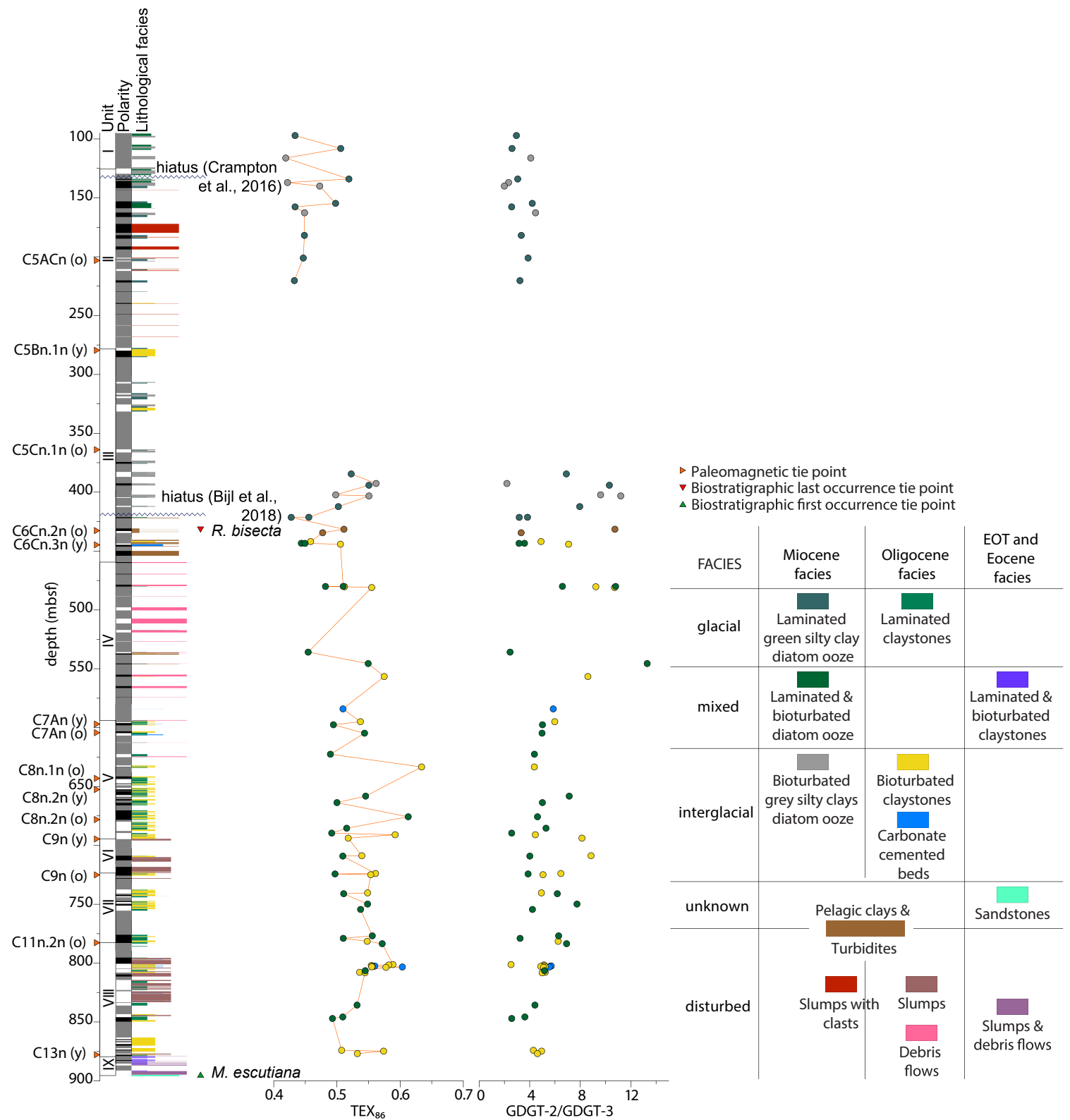
Figure 2: Lithology,TEX86 values and GDGT-2/GDGT-3 ratios of Hole U1356A plotted against depth (mbsf) with units according to Escutia et al., 2011 and chronostratigraphic tie points and paleomagnetic polarities obtained from Tauxe et al. (2012), adjusted by Crampton et al. (2016) and Bijl et al. (2018). Depositional facies and interpretation are indicated with colors following Salabarnada et al. (submitted, this volume), see legend to the right. Colors of the TEX86 and GDGT-2/GDGT-3 values reflect the lithology they have been sampled from.
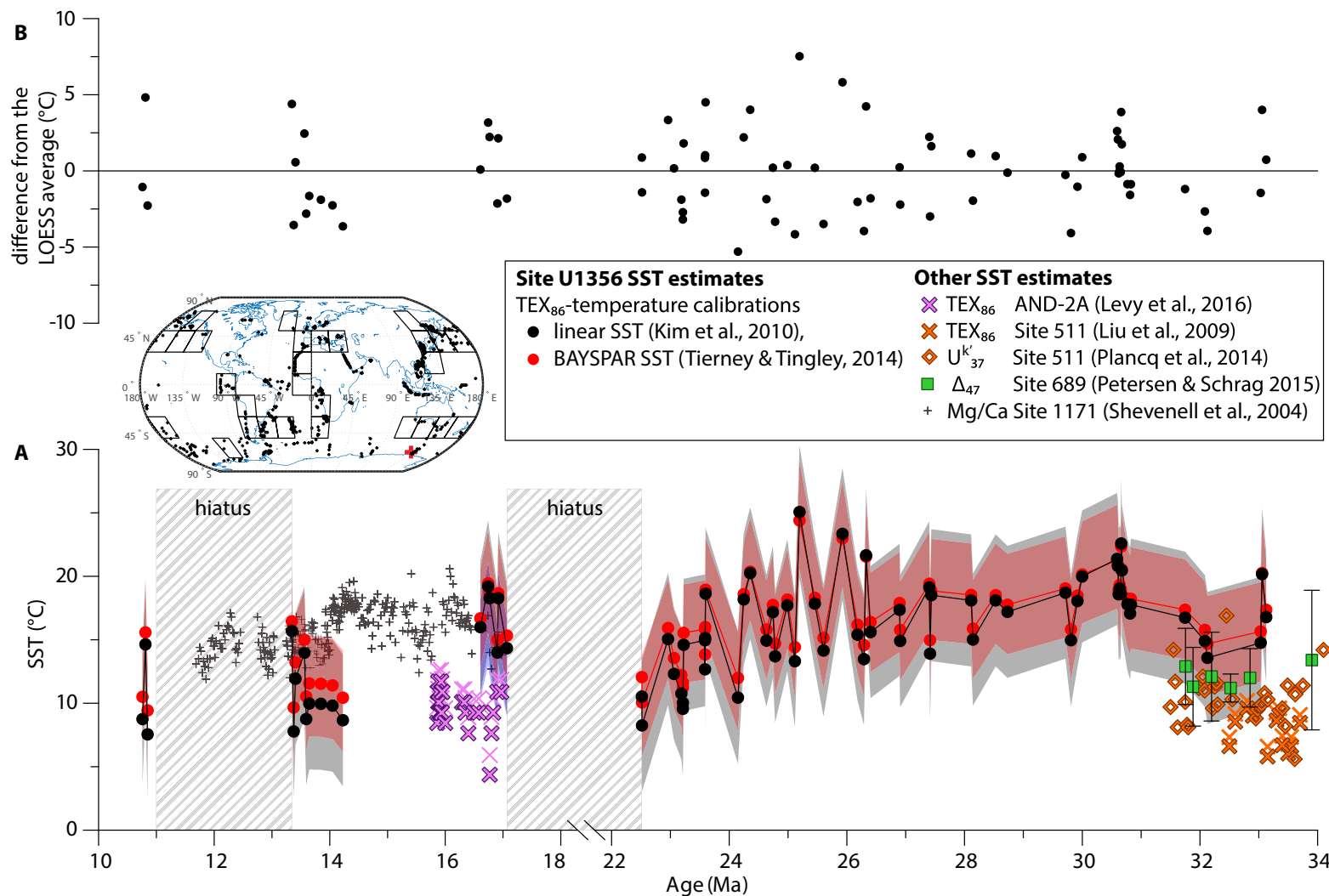
Figure 3: (A) TEX86-based SSTs plotted against age (Ma), using the linear calibration of Kim et al. (2010) and the BAYSPAR method (see text). The map (center left) indicates the 20°x20° grid cells from which core-top values (black dots) were obtained for the BAYSPAR calibration. The red + in the map indicates the location of Site U1356. Other SST estimates are plotted for comparison. For the TEX-86-based temperature estimates (purple and orange crosses), the symbols with both fill and outline are based on the linear calibration of Kim et al. (2010), those with the fill color only are based on the BAY-SPAR SST calibration (Tierney & Tingley, 2014). (B) The SST difference from the LOESS average based on the linear calibration of Kim et al. (2010) plotted against age.
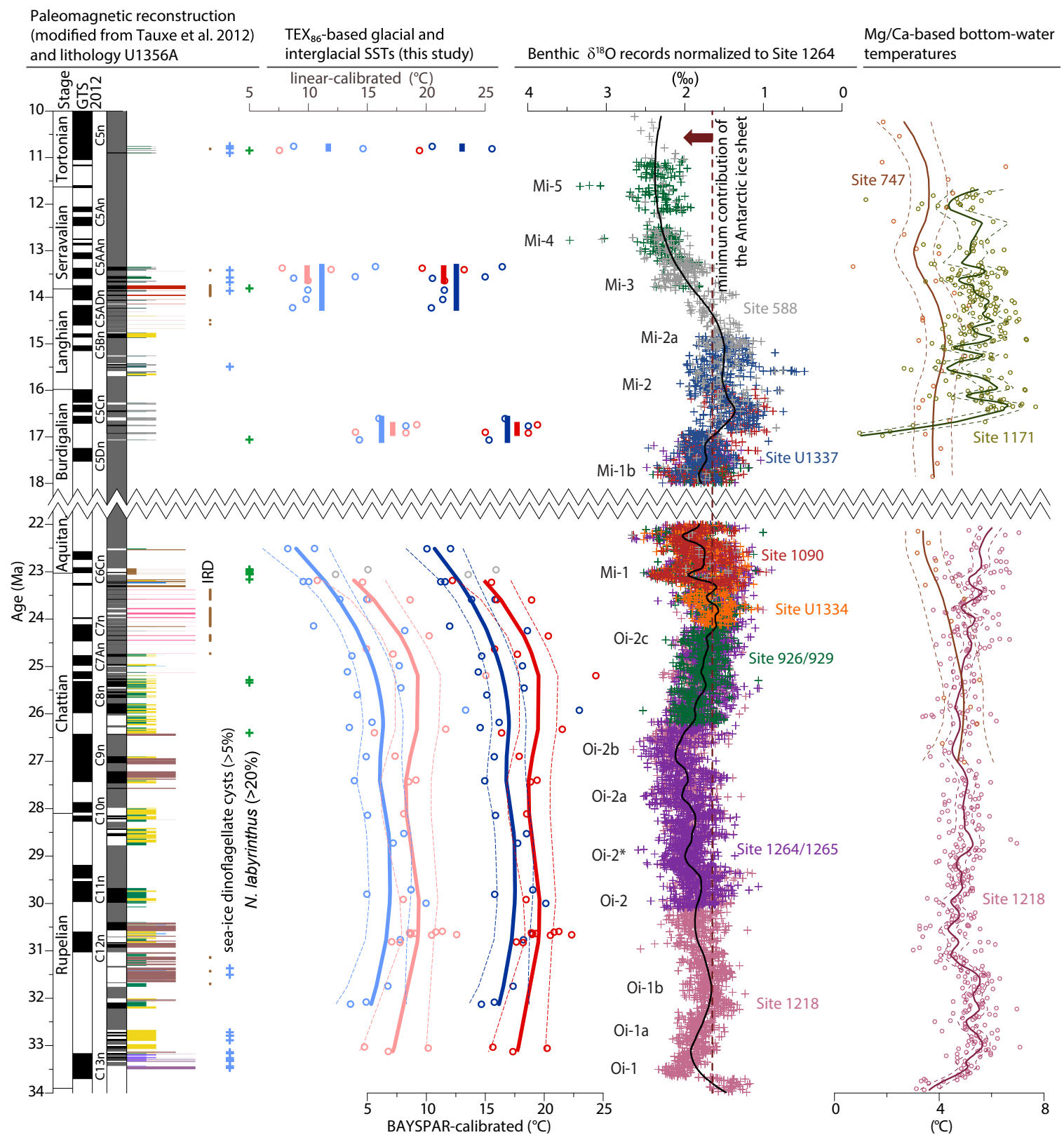
Figure 4: Lithology and paleomagnetic polarities as in Fig. 2, but plotted against age (Ma), updated to the GTS2012 timescale (Gradstein et al., 2012). Sections with IRD, and samples with sea-ice and Nematosphaeropsis labyrinthus dinoflagellate cysts are indicated. Dark colored and light colored SST values are based on the BAYSPAR calibration and linear calibration of Kim et al. (2010), respectively: (light) blue and (light) red open circles indicate glacial and interglacial temperature estimates, respectively, based on the lithology (see text). Thick (light) blue and (light) red lines are the LOESS average glacial and interglacial trends with their 95%-confidence interval (dotted lines). Benthic δ18O records are normalized to the δ18O record of Site 1264 (in purple). Colored +-signs indicate the different DSDP/ODP/IODP Sites (refs. in text) and the black line is the LOESS average. Oi- and Mi-glaciation events are indicated. The area below the benthic δ18O record on the left side of the dark red dotted line (1.65‰) indicates the minimum contribution (in ‰) of the Antarctic Ice Sheet to the benthic δ18O record, assuming BTW at Site 1264 did not drop below its modern-day value (see Liebrand et al. (2017)). Mg/Ca-based BWT records of three ODP/IODP Sites with LOESS averages (solid lines) and 95% confidence intervals (dotted lines) on the far right (refs. in text).